NASA TECHNICAL NOTE

NASA TN D-3094

NASA TN D-3094

TECH LIBRARY KAFB, NM
0130063

LOAN COPY: RETURN TO
AFWL (WLIL-2)
KIRTLAND AFB, N MEX

INTERFERENCE HEATING ON A SWEPT CYLINDER IN REGION OF INTERSECTION WITH A WEDGE AT MACH NUMBER 8

by Dennis M. Bushnell

Langley Research Center
Langley Station, Hampton, Va.

RECEIVED
20 DEC 1965
Technical Library
AF Weapons
Laboratory

NATIONAL AERONAUTICS AND SPACE ADMINISTRATION - WASHINGTON, D. C. - DECEMBER 1965

TECH LIBRARY KAFB, NM
0130063

NASA TN D-3094

INTERFERENCE HEATING ON A SWEPT CYLINDER IN REGION OF INTERSECTION WITH A WEDGE AT MACH NUMBER 8

By Dennis M. Bushnell

Langley Research Center
Langley Station, Hampton, Va.

NATIONAL AERONAUTICS AND SPACE ADMINISTRATION

For sale by the Clearinghouse for Federal Scientific and Technical Information
Springfield, Virginia 22151 – Price $2.00

INTERFERENCE HEATING ON A SWEPT CYLINDER IN REGION OF INTERSECTION WITH A WEDGE AT MACH NUMBER 8

By Dennis M. Bushnell
Langley Research Center

SUMMARY

Local heat-transfer rates and pressures have been measured on a cylinder in the interference flow region between the cylinder and a 12° half-angle wedge. The tests were conducted at a Mach number of 8 with the cylinder at sweep angles of 45° and 60° with respect to the free stream.

Comparison of the heat-transfer data with theory indicates that the boundary-layer flow changed from laminar to fully turbulent over the test Reynolds number range which was from 0.77×10^5 to 8.7×10^5 based on free-stream conditions and cylinder diameter. Tests were made with the base of the cylinder attached to and then separated from the wedge in order to investigate possible flow-separation effects in the intersection region.

Results indicate that for both sweep angles, local heating is increased along the portion of the cylinder subjected to the wedge flow, but the maximum increase can be predicted for both laminar and turbulent boundary-layer flow by using local wedge flow conditions in the infinite swept-cylinder theories of NASA TR R-104. Because of the higher local Reynolds number in the wedge flow region, transition occurs along the cylinder stagnation line at a lower value of free-stream Reynolds number for the cylinder-wedge configurations than for the undisturbed cylinder; however, the local Reynolds number for transition based on conditions ahead of the cylinder bow shock and the cylinder diameter was virtually the same for all the configurations tested.

The intersection of the wedge shock with the cylinder bow shock caused a large favorable spanwise pressure gradient along the cylinder, but no local increases in heating were observed in this region.

INTRODUCTION

Local heat-transfer rates and pressures on a body may be considerably altered by the interference flow field associated with an adjoining body. Examples of such a situation would be a wing-body juncture and the intersection region between a control surface or antenna and the supporting structure.

An interference flow with practical application to hypersonic vehicles is generated in the intersection region between a swept cylinder and a wedge. This configuration allows a simplified analysis of test results based on local flow conditions and enables an investigation of both the boundary-layer interaction problem in the intersection region itself and the shock intersection problem which occurs farther out on the cylinder.

Investigations have been made of the heating on swept leading edges attached to a long flat plate or far back on an adjoining body (refs. 1, 2, and 3). These investigations were made at a Mach number of 4.5 or less over a limited Reynolds number range. The configurations used in these references were equivalent to having the leading edge completely submerged in the flow field of the supporting body; that is, no shock impingement on the leading edge occurred.

Two previous investigations similar to the present one are reported in references 4 and 5. The configuration of reference 4 consisted of an 8° half-angle wedge with a cylinder attached at sweep angles of 20° and 60°. The tests were carried out at a Mach number of 4.15 over a Reynolds number range such that the boundary layer was always turbulent. Higher heating rates were measured in the wedge flow region, but the magnitudes could be predicted by using the turbulent theory of reference 6 and local flow conditions. Negligible effects of wedge shock impingement and no effect of flow separation on heat transfer to the cylinder was noted with the leading edge swept 60°. With the leading edge swept 20°, the large increases in pressure and heat transfer that occurred in the interference region were attributed to flow-separation effects. However, the lack of schlieren data and the fact that the wedge shock impingement was only slightly outboard of the peak heating location made separation of the effects caused by shock impingement and flow separation uncertain.

The configuration of reference 5 consisted of a 60° swept fin with a cylindrical leading edge. The fin was mounted on a flat plate and tested at a Mach number of 6. A weak shock wave which originated at the leading edge of the plate intersected the fin leading edge. The Reynolds number range of the tests was large enough so that both laminar and turbulent boundary-layer flow occurred at the stagnation line. As there were only five instrumentation locations along the cylinder stagnation line, the effects of the shock intersection and flow separation at the juncture could not be studied in detail. Also, the effects due to shock intersection could not be separated from those due to flow separation. However, the maximum measured heating rates could be predicted by using turbulent infinite-cylinder theory and local conditions.

The present investigation was undertaken to provide data for the interference region between a 12° half-angle wedge and a swept cylinder. Tests were made at a Mach number of 8 and over a Reynolds number range sufficiently large to obtain both laminar and turbulent flow. The 45° and 60° swept cylinders were provided with closely spaced instrumentation so that details of the flow-separation and shock-intersection phenomena could be obtained. Tests were made with the cylinders attached to the wedge and separated from the wedge in order to investigate separately the shock-impingement phenomena. The Reynolds number

based on free-stream conditions and cylinder diameter ranged from 0.77×10^5 to 8.7×10^5.

SYMBOLS

Measurements for this investigation were taken in the U.S. Customary System of Units. Equivalent values are indicated herein parenthetically in the International System (SI) in the interest of promoting use of this system in future NASA reports. Details concerning the use of SI, together with physical constants and conversion factors, are given in reference 7.

C_p	pressure coefficient, $\frac{p - p_\infty}{\frac{1}{2}\rho_\infty V_\infty^2}$
$C_{p,max}$	stagnation-line pressure coefficient
D	cylinder diameter, 1 in. (0.0254 m)
h	heat-transfer coefficient, $\frac{q}{T_{aw} - T_{wall}}$
$\bar{h}$	h/h_{ref}
h_{ref}	1 Btu/ft^{2}sec$^\circ$R (2.042×10^4 watts/m$^2{}^\circ$K)
L	distance from front of wedge to cylinder-wedge intersection (fig. 1(b))
l	distance along cylinder stagnation line from tip (fig. 1)
M	Mach number
N_{Pr}	Prandtl number
p	pressure
q	heating rate per unit area
R	Reynolds number
T	temperature
V	velocity
β	velocity gradient parameter (ref. 6)
ϕ	angular distance around cylinder in chordwise plane measured from stagnation line (fig. 2)

θ'_{wall} gradient of enthalpy profile parameter at wall (ref. 6)

Λ sweep angle, measured from cylinder bow shock to perpendicular to local flow direction (fig. 1)

ρ density

Subscripts:

aw adiabatic wall

D cylinder diameter

e local external to boundary layer

s stagnation line

ω wedge flow

wall cylinder wall

∞ tunnel free stream

o tunnel stagnation

APPARATUS

Tunnel

Testing of the models was conducted in the Langley Mach 8 variable-density tunnel. This tunnel is of the blowdown type and has an axially symmetric nozzle with contoured walls. The average test-section Mach number variation with stagnation pressure ranges from 7.80 to 7.96 for values of stagnation pressure from 200 to 1000 psi gage (1.379 to 6.895 MN/m^2 gage). (See ref. 8.) A Mach number of 8 was assumed for the highest stagnation pressure tested, which was 2600 psi gage (17.9 MN/m^2 gage), as the tunnel calibration presently available does not extend to this value. For the present tests the stagnation temperature varied from 840° F to 1000° F (722° K to 811° K). The range of test-section Reynolds number based on the 1-inch (0.0254-m) diameter of the cylinder and free-stream conditions was from 0.77×10^5 to 8.7×10^5.

Models

General description.- The models used consisted of a sharp flat plate inclined at a 12° angle to the test-section flow, thereby forming a 12° half-angle wedge, and circular cylinders either attached to or separated from the wedge and swept at 45° and 60° with respect to the free stream. A side view

of the test configuration where the cylinder and wedge are separated is shown in figure 1(a). The 12° half-angle wedge, 8 inches (0.20 m) wide and 19 inches (0.48 m) long, was made of type 347 stainless steel. The wedge was supported by a strut attached to the top portion of the test section and was in position when the tunnel was started. The 1-inch-diameter (0.025-m) cylinders were constructed of type 347 stainless steel, and were provided with an elliptically shaped end plate. The end of the cylinder and the end plate were parallel to the local wedge flow for both sweep angles.

Shown in figure 1(b) is a side view of the test configuration where the cylinder and wedge are attached. The same wedge and cylinders were used, but the end plate was removed and the cylinder was attached directly to the wedge. The length of the cylinder was reduced for this configuration. The cylinder was attached to the wedge 1.5 inches (0.038 m) off the center line of the wedge in order to avoid weak center line disturbances in the axisymmetric nozzle.

In order to provide reference values, the cylinders were tested without the wedge, but with the same end plate as shown in figure 1(a) inclined into the flow at 12°. Thus undisturbed infinite-cylinder data were obtained, except in the region near the end plates.

Instrumentation.- Four different cylinder models were constructed; two for each of two sweep angles, 45° and 60°. Two of the cylinders were machined with a wall thickness of 0.030 inch (0.0008 m) and served as heat-transfer models. The instrumentation locations were identical for both the heat-transfer and the pressure models and are shown in figure 2. The thermocouples were installed by drilling a 0.026-inch (0.0007-m) hole through the skin, inserting and soldering the ends of a No. 30 gage iron-constantan thermocouple (0.010-inch-diameter (0.0003-m) wire), and fairing the region flush with the surrounding surface. The other two cylinders were made with a wall thickness of 0.0625 inch (0.002 m) and were instrumented with pressure orifices. The ends of the 0.040-inch (0.001-m) inside-diameter monel tubing used were silver soldered flush with the surface of the model. The wedge was not instrumented.

Equipment

The temperature-time history of the model was recorded on magnetic tape with an analog to digital data recorder system. A digital computing machine was used to reduce the temperature data to heating rates. The pressure data were recorded photographically from mercury manometers. Tunnel stagnation pressure was measured with a Bourdon tube gage.

TEST PROCEDURES AND DATA REDUCTION

The heat-transfer data were obtained by the transient heating technique. For this technique steady flow was established in the test section with the model outside the tunnel; the model was then injected into the test-section flow for the test period, which was about 4 seconds in duration. The model was then removed and brought to isothermal conditions at approximately room

temperature in preparation for another test. The time required to move the model through the tunnel boundary layer was about 0.05 second, and care was taken to eliminate this effect from the data.

For tests of the configuration with the cylinder and wedge separated, only the cylinder was injected, but for tests of the configuration with the cylinder and wedge attached, the entire model was injected.

The temperature data were reduced to heating rates on a digital computing machine. Details of data reduction methods used may be found in reference 9. In order to obtain values of the heat-transfer coefficient, a recovery factor of 0.85 was assumed for laminar boundary-layer flow, and 0.89 for transitional or turbulent flow. The recovery factor is defined as $\left(T_{aw} - T_e\right)/\left(T_o - T_e\right)$.

The pressure data were also taken by injecting the model into the test section after the tunnel was started, but the testing time was of the order of 30 seconds to allow settling out time for the mercury manometers.

ACCURACY

Heat-Transfer Data

The accuracy of the heat-transfer data obtained by means of the automatic data-reduction system is a function of the heating rates being measured. Because of errors in this system and the possibility of additional errors in measured temperatures, skin thickness, and the values of density and specific heat of the material used, the final heat-transfer-coefficient data are probably accurate to within 15 percent.

Pressure Data

The accuracy of the pressure data is determined by the accuracy within which the manometer data can be read from the film. The percent error is a function of the pressure level being measured since the absolute error is about 0.01 inch (0.0003 m) of mercury. Because of these reading errors and also because of the possibility of errors in tunnel stagnation pressure, the final data are accurate to within 5 percent.

RESULTS AND DISCUSSION

Flow Field

Shown in figure 3 are schlieren photographs for the configurations with the cylinder swept back 45° with respect to the free stream. Figure 3(a) is a schlieren photograph of the undisturbed cylinder and shows that the bow shock becomes parallel to the swept cylinder about 2 to 3 diameters from the tip.

Figure 3(b) is a photograph of a test with the cylinder and wedge separated and figure 3(c) is a photograph of a test with the cylinder and wedge attached. The structures of these flow fields can best be explained by considering two-dimensional theory for the intersection of two shocks.

Shown in figure 4 is a schematic sketch of the inviscid two-dimensional flow field associated with the intersection of two shocks of the same family (ref. 10). The case shown corresponds to that of the cylinder and wedge attached as in figure 3(c). The cylinder bow shock and the two-dimensional wedge shock intersect at point A. An extension of the cylinder bow shock continues downstream between regions 1 and 5, and is deflected away from the cylinder. A vortex sheet originates at point A and forms the boundary between regions 4 and 5. Expansion waves emanate from point A, impinge on the cylinder, and are reflected back; thus they interact with the continuation of the cylinder bow shock and turn this shock back toward the cylinder. If two-dimensional flow is assumed, the expansion from region 3 to region 4 must fulfill the criteria that the static pressures are equal and that the flow directions are the same in regions 4 and 5. The expansion impingement on the cylinder causes a favorable spanwise pressure gradient. Region 6 is therefore a region of low pressure, which should be approximately equal to the pressure on an undisturbed cylinder at the local sweep angle subjected to the test-section flow.

In figure 3(b) it can be seen that the two shocks intersect and that the cylinder bow shock is deflected away from the cylinder. A vortex sheet emanates from the intersection region. The line which appears where the expansion waves should be is the continuation around the cylinder of the two-dimensional wedge shock. However, the effect of the expansion waves can be seen where the bow shock is deflected back toward the cylinder. Also, the vortex sheet changes direction because of the passage of the reflected expansion waves.

The separation distance between the cylinder and the wedge was 0.63 inch (0.016 m) and was larger than the local wedge boundary-layer velocity thickness, which for the lowest unit Reynolds number was calculated by the method of reference 11 to be 0.15 inch (0.004 m) at a distance of 1 foot (0.305 m) from the wedge leading edge. Therefore, the wedge boundary layer should not affect the flow over the cylinder. Figure 3(c), which is for the cylinder and wedge attached, shows the same flow characteristics as figure 3(b). Comparison of figures 3(a) and 3(b) shows that the standoff distance of the cylinder bow shock is always larger, within the field of view, for the wedge-interference configuration than for the cylinder only. Presumably this difference would decrease with increasing spanwise distance from the disturbance.

Figure 5 is a set of photographs similar to figure 3, but for the configurations with the cylinder swept back 60°. Inasmuch as the flow patterns shown in this figure for the 60° swept cylinders are similar to those shown in figure 3 for the cylinders with 45° of sweep, the remarks made for figure 3 apply for this figure also. That is, the flow field is similar to what would be expected from two-dimensional shock-intersection theory. Again the bow shock standoff distance for the interference configuration is larger than that for the cylinder only. The photograph shown in figure 5(c) and data from other tests indicate that there was negligible flow separation at the cylinder-wedge juncture for $\Lambda_\infty = 60°$.

Shown in figure 6 are schlieren photographs of the wedge-cylinder intersection region for $\Lambda_\infty = 45^\circ$. The photographs are arranged in order of increasing Reynolds number from $R_{\infty,D} = 0.94 \times 10^5$ to $R_{\infty,D} = 3.51 \times 10^5$. A region of flow separation which apparently causes the oblique shock, as indicated by the arrow, can be seen in figure 6(a). As the Reynolds number is increased, the extent of flow separation decreases as evidenced by the location of the oblique shock, until at a value of $R_{\infty,D}$ of about 3.05×10^5 the flow appears to be fully attached at the wedge-cylinder juncture. At the lower Reynolds numbers there is sufficient flow separation to affect the first thermocouple along the cylinder.

Pressure Distributions

Spanwise.- Shown in figure 7 are the pressure distributions along the stagnation line of the cylinders swept at 45°. The data are given as ratios of the local measured pressures to tunnel stagnation pressures. Figure 7(a) shows the results for the undisturbed cylinder (that is, the wedge is not in the flow) and for the wedge and cylinder attached. Two calculated pressure levels are shown on this plot. The level on the right is calculated by assuming an infinite swept cylinder subjected to the test-section flow. The level shown on the left is calculated by assuming a cylinder subjected to the wedge flow field and swept parallel to the cylinder bow shock as measured before the intersection point (Λ_ω in fig. 4). This measured shock angle gave a sweep angle of 53° with respect to the local wedge flow. Indicated at the bottom of figure 7 are the measured shock-intersection location and the calculated expansion-impingement region obtained by assuming the two-dimensional flow field shown in figure 4 and using the measured shock standoff distance. Measurements for the undisturbed cylinder (no wedge flow) are included on these plots to indicate that the disturbed values do approach the measured infinite-cylinder values downstream of impingement, in spite of the larger shock standoff distance for the disturbed case.

In this figure it can be seen that the pressure is higher in the region of the cylinder which is subjected to the wedge flow than in the region which is affected by the test-section flow. The levels are in approximate agreement with the theoretical values. The expansion impingement on the cylinder causes a large favorable spanwise pressure gradient in agreement with the postulated flow mechanism of figure 4. The flow then overexpands before increasing to the infinite swept-cylinder value.

Because of end effects the measured sweep angle Λ_ω used for the wedge flow region is less than the geometric sweep angle, which is $45^\circ + 12^\circ$, or 57°. Therefore, the calculated and measured pressure levels are higher than the levels for a cylinder at the geometrical sweep angle. The following method could be used to obtain a conservative estimate of this pressure level in the interference region for design purposes: If the shock standoff distance for the cylinder subjected to the test-section or undisturbed flow and the wedge shock location are known, a shock intersection point can be found. Then if a shock is drawn from this intersection point to the cylinder-wedge junction, it

will represent a lower limit on the local sweep angle and therefore an upper limit on the pressure which could occur inboard of the shock impingement. Application of this procedure to the case of figure 7(a), for example, gives $\Lambda_\omega = 46^\circ$, and results in a pressure ratio of 0.013.

Figure 7(b) shows results for the case of the cylinder and wedge separated. The essential features of the distribution shown in this figure are the same as those of figure 7(a). Comparison of figures 7(a) and 7(b) shows that there is no marked difference between the results for the cylinder-attached and cylinder-separated cases. The first data point in the cylinder-attached plot (fig. 7(a)) is high, but this station was probably affected by the separation phenomena discussed in connection with the schlieren photographs of figure 6. Also, the mean pressure in the wedge flow region (excluding the point of $l/D = 0.55$ in fig. 7(a)) is higher in figure 7(b) than in figure 7(a). This difference in pressure could be explained by the fact that the cylinder bow shock forms more nearly normal to the wedge flow for the cylinder-separated case, where a small end plate is present, than for the attached case, where the shock is influenced by the wedge boundary layer (figs. 3(b) and 3(c)).

Shown in figure 8 are the spanwise pressure distributions obtained for the configurations with the cylinder swept back 60°. Figure 8(a) shows the results for the wedge and cylinder attached, and figure 8(b), for the wedge and cylinder separated. The distributions obtained are similar to those for the $\Lambda_\infty = 45^\circ$ configurations except that, because of the increase in sweep angle, the wedge shock impinges farther out on the cylinder. Comparison of figures 8(a) and 8(b) indicates that for $l/D \leqq 1.55$ the pressures for the cylinder separated (fig. 8(b)) are higher than those for the cylinder attached (fig. 8(a)). This difference was probably due to the same shock angle effect discussed in connection with figures 7(a) and 7(b). For figure 8 the theoretical level in the wedge flow region was computed in the same manner as for figure 7, with the sweep angle of the cylinder bow shock being 68° with respect to the wedge flow. Agreement of the data with theoretical pressure levels is generally good.

Chordwise.- Shown in figures 9 to 11 are the results of the chordwise pressure measurements. Figure 9 presents the data for the undisturbed cylinders for both $\Lambda_\infty = 45^\circ$ and $\Lambda_\infty = 60^\circ$. Data are shown for three spanwise stations. The ratio $C_p/C_{p,max}$ was formed at each spanwise station by using the measured stagnation-line pressure for $C_{p,max}$ at that station; therefore, by definition, $C_p/C_{p,max} = 1.0$ at $\phi = 0^\circ$ at all spanwise stations. Also shown in this figure is the Newtonian pressure distribution, $C_p/C_{p,max} = \cos^2\phi$. The station for $\Lambda_\infty = 60^\circ$ at $l/D = 1.05$ and $\phi = 60^\circ$ is closer to the end plate than the corresponding station for $\Lambda_\infty = 45^\circ$. Therefore the high point at this position in figure 9(b) is probably due to interference from the end plate, which, for the undisturbed cylinder, was not alined with the flow.

Shown in figure 10 are the data for the $\Lambda_\infty = 45^\circ$ wedge-cylinder configuration. In figure 10(a) the data for $l/D = 1.05$ and $l/D = 3.55$ at $\phi = 30^\circ$ are in agreement with Newtonian theory, while at $\phi = 60^\circ$ the data are higher than the theory. The measurements at $l/D = 2.05$ are considerably above the theory at both $\phi = 30^\circ$ and $\phi = 60^\circ$. The reason for this effect is as follows:

The stagnation-line pressure distributions corresponding to figure 10(a) are shown in figure 7(a). The $l/D = 2.05$ station is in the region of the spanwise gradient, which is caused by the expansion waves which emanate from the shock-intersection region. Inasmuch as these waves are at an angle to the cylinder, they will impinge on the cylinder at a smaller value of l/D at the stagnation line ($\phi = 0^\circ$) than at stations where $\phi > 0^\circ$. Therefore the pressure-coefficient value at $\phi = 0^\circ$ has been affected by the expansion, whereas the values at $\phi = 30^\circ$ and $\phi = 60^\circ$ at the same l/D station have not. This effect causes a lower value of $C_{p,max}$, which results in values of the pressure-coefficient ratio greater than 1 at $\phi = 30^\circ$, as seen in figure 10(a).

In figure 10(b) the $l/D = 2.05$ station is farther outboard from the shock-intersection region and therefore the expansion has already lowered the pressure at $\phi = 30^\circ$. At $\phi = 60^\circ$, however, a small effect similar to that apparent in figure 10(a) is seen and is probably caused by the same phenomenon.

The chordwise distributions for the configurations with the cylinder swept back 60° are shown in figure 11. As seen in figure 8, the $l/D = 3.55$ station is now the one in the expansion-impingement region, and the measured pressure values at $l/D = 3.55$ therefore show the same trends exhibited at $l/D = 2.05$ in figure 10.

Heat-Transfer Data

Spanwise distribution.- Shown in figure 12 are typical heat-transfer distributions for the undisturbed cylinder at sweep angles of 45° and 60°. The two distributions shown are for $R_{\infty,D} = 2.55 \times 10^5$. Also shown in this figure are the infinite-cylinder values calculated by using the method of reference 6 for both laminar and turbulent stagnation-line boundary-layer flow. For turbulent flow, the reference temperature which appears in the theory was assumed to be the local value external to the boundary layer, and the values of n and a (parameters in the skin-friction law) suggested in reference 6 were used (that is, $n = 4$ and $a = 0.0228$). In all the heat-transfer-coefficient calculations, the theoretical pressure levels shown in figures 7 and 8 were used.

Figure 12(a) presents a distribution for the configuration with the cylinder swept back 45° at $R_{\infty,D} = 2.55 \times 10^5$. The fact that the data fall between the two theoretical levels probably indicates that at this Reynolds number the stagnation-line boundary layer is transitional. The variations in the data for small values of l/D are probably due to end effects.

Figure 12(b) shows a distribution for $\Lambda_\infty = 60^\circ$, at $R_{\infty,D} = 2.55 \times 10^5$, and the agreement of the data with the theoretical turbulent level indicates that the stagnation-line boundary layer is turbulent at this Reynolds number. The low value of heat-transfer coefficient on the left of the curve could be caused either by end effects or by a tendency to retain laminar flow in this region. That is, the cylinder stagnation-line boundary layer at a 60° sweep angle may require a finite spanwise distance to become turbulent.

Shown in figure 13 are typical spanwise heat-transfer distributions for the wedge-cylinder configurations with the cylinder swept back 45°. Figure 13(a) shows distributions for the wedge and cylinder attached at a free-stream Reynolds number of 2.66×10^5. There are two flow regimes present, one of which is due to the wedge flow field and affects the end portion of the cylinder, and the other of which is due to the test-section flow and affects the portion of the cylinder beyond the shock-impingement region. The theoretical levels shown were calculated by applying the theory of reference 6 and the local conditions associated with each of the flow fields.

The values of l/D for shock intersection and calculated expansion impingement are indicated by vertical lines in figure 13(a). Also shown is the approximate location of the vortex-sheet impingement. The heat-transfer data are in agreement with the theory in the wedge flow region, but then seem to decrease with the pressure level (see fig. 7(a)), in that they follow the overexpansion which occurs in the pressure and then return to the undisturbed-cylinder level. The measured values fall below the theory after the impingement of the vortex sheet. No increase in heating is apparent in the shock-intersection region aside from the higher values associated with the wedge flow region. These wedge flow values can be adequately predicted, as indicated by the agreement between the turbulent theory and the data. This agreement indicates that the stagnation-line boundary layer is turbulent at $R_{\infty,D} = 2.66 \times 10^5$. It should be noted that the wedge Reynolds number $\left(R_{w,D}\right)$ is higher than the test-section value, and therefore transition for interference flow would be expected to occur at a lower value of free-stream Reynolds number $\left(R_{\infty,D}\right)$ than for an undisturbed cylinder.

The data point at $l/D = 0.55$ may have been affected by the reimpingement of separated flow in the cylinder-wedge intersection region, which was discussed previously in connection with figure 6.

Figure 13(b) presents the data for the cylinder and wedge separated at approximately the same Reynolds number as that of figure 13(a). The data follow the same type of distribution as in figure 13(a). The general level can be predicted by the theory and again no large increase in h_s is apparent in the shock-impingement region.

Shown in figure 13(c) are the data for a lower Reynolds number than that of figures 13(a) and 13(b) with the wedge and cylinder separated. Comparison of the data with theory indicates that the boundary layer was always laminar. Comparison of figures 13(b) and 13(c) indicates that the conclusions reached from the turbulent distribution can also be applied to the laminar. The conclusions are as follows: there is no apparent increase in heating due to shock impingement; heating is higher on the cylinder in the wedge region than on the undisturbed cylinder; and the general heating levels can be calculated by using infinite swept-cylinder theory with appropriate local conditions.

Figure 14 presents a set of results similar to those presented in figure 13 but for the wedge-cylinder configurations with the cylinder swept back 60°. Figure 14(a) gives data for the wedge and cylinder attached. The data in this

figure are above the theory in the wedge region but are in fair agreement in the undisturbed region. The flow is turbulent, and no increase in heating occurs in the shock-impingement region. Figure 14(b) presents results for the cylinder and wedge separated at approximately the same Reynolds number. The agreement with theory in the wedge flow region is much better in figure 14(b) than in figure 14(a), but the flow seems to require about 1.5 inches (0.038 m) of spanwise flow before the turbulent level is achieved. The reason that the data are above the theory in figure 14(a) and are in agreement with the theory in figure 14(b) is not understood. The difference between the pressure data for the wedge flow region in figures 8(a) and 8(b) is not great but indicates, if anything, that the data for figure 14(b) should be above the theory and that the data for figure 14(a) should be in agreement with the theory. However, the opposite phenomena actually occurred.

Shown in figure 14(c) is a distribution for the wedge and cylinder separated, at a lower Reynolds number than that of figures 14(a) and 14(b). Comparison of data with theory indicates that the boundary layer was laminar. Again, as in the laminar distribution for $\Lambda_\infty = 45^\circ$, no increase in heating is apparent in the shock-impingement region, and the general levels can be predicted, although in this figure the data are below the theory in both regions.

Figure 15 presents a comparison of heat-transfer-coefficient distribution along the cylinder stagnation line for the undisturbed cylinder and for the cylinder and wedge separated. Tests were made for $\Lambda_\infty = 45^\circ$ at approximately the same Reynolds number for the two cases. At this free-stream Reynolds number the upper portion of the disturbed cylinder encounters a high enough local Reynolds number in the wedge flow region for the flow to become turbulent. After shock intersection and expansion impingement, the stagnation-line boundary layer remains turbulent but shows a tendency at large values of l/D to revert to the laminar level.

At the same free-stream Reynolds number the heating level for the undisturbed cylinder is slightly higher than the theoretical laminar value. Therefore this comparison indicates that once the stagnation-line boundary layer becomes turbulent, the turbulence seems to propagate down the stagnation line into the portion of the cylinder which is subjected to the lower Reynolds number test-section flow.

Correlation of stagnation-line heat-transfer coefficients with Reynolds number.- Shown in figures 16 and 17 are stagnation-line heat-transfer coefficients plotted as a function of local Reynolds number for the flow upstream of the cylinder bow shock at given values of l/D. These plots should give an indication concerning the agreement between the theory and the data, and also should serve to present a more unified picture concerning the state of the stagnation-line boundary layer, that is, whether it is laminar or turbulent. Figure 16 presents the data for $\Lambda_\infty = 45^\circ$ while figure 17 shows the data for $\Lambda_\infty = 60^\circ$.

Although the stagnation temperature for different configurations shown in figures 16 and 17 varied from 850° F to 1000° F (727° K to 811° K), this

variation caused only slight deviations in the theoretical values of h_s, and, therefore, only one line is shown for each theory, laminar and turbulent.

Figure 16(a) shows the heat-transfer coefficient in the wedge flow region at $l/D = 1.05$ plotted as a function of wedge-flow Reynolds number. The data are in good agreement with the theory for both the separated and attached configurations. The value of wedge Reynolds number where transition begins to occur is seen to be about 1.3×10^5.

Shown in figure 16(b) are results obtained in the undisturbed region at $l/D = 4.3$. The abscissa is the test-section Reynolds number based on the 1-inch (0.025-m) cylinder diameter. Again the data are in reasonable agreement with the theory. The stagnation-line boundary layer for the undisturbed cylinder remains laminar up to a value of $R_{\infty,D}$ of about 1.4×10^5, whereas the boundary layers for the interference flows become transitional at a value of $R_{\infty,D}$ of about 1×10^5. For the values of $R_{\infty,D}$ where the undisturbed cylinder flow is laminar, the flow on the cylinder in the wedge region is already turbulent because of the higher local Reynolds number there. This turbulence seems to propagate down the cylinder into the undisturbed flow region, as discussed in connection with figure 15.

Also shown in figure 16(b) is a dashed line which represents turbulent theory for which the wall temperature (100° F (311° K)) instead of the local temperature external to the boundary layer was used as the reference temperature. The theory which used T_e as the reference temperature is seen to be in better agreement with the data.

Shown in figure 17(a) are the data obtained in the wedge flow region at $l/D = 2.05$ for the configurations with the cylinder swept back 60°. The values for the cylinder and wedge attached are above the curve calculated by theory, as discussed in connection with figures 14(a) and 14(b), except at the highest value of $R_{\omega,D}$. However, the difference is only about 10 percent. Approximately the same value of transition Reynolds number as that for the configuration with the cylinder swept back 45° is apparent in this figure $\left(R_{\omega,D} \approx 1.3 \times 10^5\right)$.

Figure 17(b) presents the data in the undisturbed flow region at $l/D = 5.3$. For the undisturbed cylinder, the transition Reynolds number seems to be approximately 1.4×10^5. Again, this value is close to that for the undisturbed cylinder swept back 45° and also close to the value of 1.3×10^6 for the wedge flow region. It therefore appears that, at Mach 7.95 or 5.3 (wedge flow) and over the range of effective sweep angle from 45° to 68°, a value of about 1.4×10^5 is reasonable to assume for a transition Reynolds number for swept cylinders in terms of local flow conditions ahead of the bow shock. The cylinder and wedge data exhibit the same reduction in free-stream transition Reynolds number noted previously in figure 16(b).

The agreement of the data with theory in figure 17(b) is good. A dashed turbulent-theory line which assumed T_{wall} as the reference temperature is also

shown in this figure. The choice in this figure between using T_e or T_{wall} as the reference temperature is not as clear-cut as it was in figure 16(b).

Chordwise distribution.- Shown in figures 18 to 20 are typical chordwise heat-transfer distributions. Figure 18 presents the data from tests on the undisturbed cylinder for both sweep angles and for both laminar and turbulent stagnation-line boundary-layer flow. The theoretical distributions shown were computed by using the method of reference 6 where, for laminar flow $\left[\frac{\theta_w'}{(\theta_w')_{\beta=1}}\right]_{N_{Pr}=1} = 1$ was assumed. In reference 6, θ_w' is the gradient of the enthalpy profile parameter at the wall. This assumption was made since the values of β are all greater than 1 and therefore only a 3 to 4 percent error is involved. The measured heat-transfer coefficients have been nondimensionalized with respect to the measured stagnation-line value at the same l/D station. Thus $h/h_s = 1$ for all stations at $\phi = 0^\circ$. Inasmuch as the agreement obtained between measured and Newtonian chordwise pressure distributions was good, the Newtonian values were used in the application of the theory.

Figure 18(a) presents the data for a test with a laminar stagnation-line boundary layer and a sweep angle of 60°. The $l/D = 1.05$ station is the one closest to the end plate, and therefore, the difference between the theory and the data at this station is probably due to end effects. These data are shown to indicate the maximum end effects which were measured. The data at the other two stations are slightly below the calculated laminar distribution. Figure 18(b) presents data for the same sweep angle but for a turbulent stagnation-line boundary layer. Again, the $l/D = 1.05$ station is disturbed by end effects, and therefore, these data do not agree with measurements at the other two stations. The turbulent theory in figure 18(b) underpredicts the data; at $\phi = 60^\circ$ the theory is 20 percent below the data. A similar trend is shown in reference 6 for the same sweep angle. The data of the investigation of reference 6 are about 28 percent above the theory at $\phi = 60^\circ$. In figure 18(c) are shown data for a laminar boundary layer and a sweep angle of 45°. Again, there is good agreement between the laminar theory and the data.

Figures 19 and 20 present data for the cylinder and wedge attached. The data shown in figure 19 are for a sweep angle of 45° with respect to the free-stream flow. Figure 19(a) shows the distribution for a laminar stagnation-line boundary layer, and the data, both in the wedge flow region and downstream of expansion impingement, agree well with the theoretical distribution. Figure 19(b) presents data for a transitional stagnation-line boundary layer. A comparison of the data with the laminar- and turbulent-theory distributions shown in this figure indicates that the measured values are better represented by the turbulent distribution than by the laminar distribution. In the discussion of the chordwise pressure distributions (fig. 10(a)), it was noted that the expansion waves intersect the cylinder at an angle, and therefore at the same l/D station, the pressure level at the stagnation line could be below that at some angle ϕ around the cylinder. If this same explanation is applied to the heat-transfer measurements, the reason for the high data point at $l/D = 2.05$ and $\phi = 30^\circ$ is easily understood.

Shown in figure 20 are data for a turbulent stagnation-line boundary layer for both sweep angles. Figure 20(a) presents distributions for $\Lambda_\infty = 45^\circ$. Again, as for the undisturbed cylinder, the theory is about 20 percent below the data at $\phi = 60^\circ$. The $l/D = 2.05$ station is in the shock-impingement region, and therefore, the high data point at this station at $\phi = 30^\circ$ is understandable in light of the discussion of figure 19(b).

Similar trends are seen for the data for $\Lambda_\infty = 60^\circ$ shown in figure 20(b); that is, the data are about 20 percent above the turbulent theory at $\phi = 60^\circ$, and the data in the expansion-impingement region ($l/D = 3.55$) are higher than at the other stations.

CONCLUSIONS

Local heat-transfer rates and pressures have been measured on a 1-inch-diameter cylinder in the interference flow region between the cylinder and a 12° half-angle wedge. The tests were conducted at a Mach number of 8 with the cylinder at sweep angles of 45° and 60° with respect to the free stream. The test Reynolds number, based on free-stream conditions and cylinder diameter, ranged from 0.77×10^5 to 8.7×10^5. Tests were made on configurations with the base of the cylinder attached to the wedge and separated from the wedge, and also on the cylinder alone.

The following conclusions can be made:

1. For both sweep angles local heating is increased along the portion of the cylinder subjected to the wedge flow, but the maximum increase can be predicted for both laminar and turbulent stagnation-line flow by using local conditions in the infinite swept-cylinder theories of NASA TR R-104.

2. The theory for turbulent heating on infinite cylinders appeared to agree better with the data if the local temperature external to the boundary layer was used as the reference temperature.

3. The extent of the flow separation in the cylinder-wedge juncture was small for the present test conditions, and therefore, in the region of the measuring stations, there was no appreciable difference between the data for the cylinder attached and cylinder separated.

4. No local increases in heating were measured in the region of the wedge shock impingement for either laminar or turbulent stagnation-line boundary-layer flow.

5. The wedge flow caused transition to occur at a lower value of free-stream Reynolds number for the cylinder-wedge configurations than for an undisturbed cylinder. However, if the local wedge Reynolds number is used as a criteria for the wedge-cylinder tests, transition occurred both with and without the wedge flow present at a value of local Reynolds number ahead of the cylinder bow shock of about 1.4×10^5 based on cylinder diameter.

6. When the wedge flow caused transition for the wedge-cylinder configurations at a smaller value of free-stream Reynolds number than for the undisturbed cylinder, then increased heating characteristic of turbulent boundary layers persisted all the way along the cylinder for both sweep angles of 45° and 60°.

7. Comparison of the chordwise heat-transfer data with infinite swept-cylinder theory indicates that the theoretical turbulent distribution underpredicts the data by 20 percent at 60° around the cylinder.

Langley Research Center,
National Aeronautics and Space Administration,
Langley Station, Hampton, Va., July 29, 1965.

REFERENCES

1. O'Neal, Robert L.; and Bond, Aleck C.: Heat Transfer to 0° and 75° Swept Blunt Leading Edges in Free Flight at Mach Numbers From 1.90 to 3.07. NASA TN D-1256, 1962. (Supersedes NACA RM L58A13.)

2. Burbank, Paige B.; Newlander, Robert A.; and Collins, Ida K.: Heat-Transfer and Pressure Measurements on a Flat-Plate Surface and Heat-Transfer Measurements on Attached Protuberances in a Supersonic Turbulent Boundary Layer at Mach Numbers of 2.65, 3.51, and 4.44. NASA TN D-1372, 1962.

3. Price, Earl A.; Howard, Paul W.; and Stallings, Robert L., Jr.: Heat-Transfer Measurements on a Flat Plate and Attached Fins at Mach Numbers of 3.51 and 4.44. NASA TN D-2340, 1964.

4. Beckwith, Ivan E.: Experimental Investigation of Heat Transfer and Pressures on a Swept Cylinder in the Vicinity of Its Intersection With a Wedge and Flat Plate at Mach Number 4.15 and High Reynolds Numbers. NASA TN D-2020, 1964.

5. Jones, Robert A.: Heat-Transfer and Pressure Investigation of a Fin-Plate Interference Model at a Mach Number of 6. NASA TN D-2028, 1964.

6. Beckwith, Ivan E.; and Gallagher, James J.: Local Heat Transfer and Recovery Temperatures on a Yawed Cylinder at a Mach Number of 4.15 and High Reynolds Numbers. NASA TR R-104, 1961. (Supersedes NASA MEMO 2-27-59L.)

7. Mechtly, E. A.: The International System of Units - Physical Constants and Conversion Factors. NASA SP-7012, 1964.

8. Stainback, P. Calvin: Heat-Transfer Measurements at a Mach Number of 8 in the Vicinity of a 90° Interior Corner Alined With the Free-Stream Velocity. NASA TN D-2417, 1964.

9. Stainback, P. Calvin: Heat-Transfer Measurements at a Mach Number of 4.95 on Two 60° Swept Delta Wings With Blunt Leading Edges and Dihedral Angles of 0° and 45°. NASA TN D-549, 1961.

10. Shapiro, Ascher H.: The Dynamics and Thermodynamics of Compressible Fluid Flow. Vol. I. The Ronald Press Co., c.1953.

11. Beckwith, Ivan E.; and Cohen, Nathaniel B.: Application of Similar Solutions to Calculation of Laminar Heat Transfer on Bodies With Yaw and Large Pressure Gradient in High-Speed Flow. NASA TN D-625, 1961.

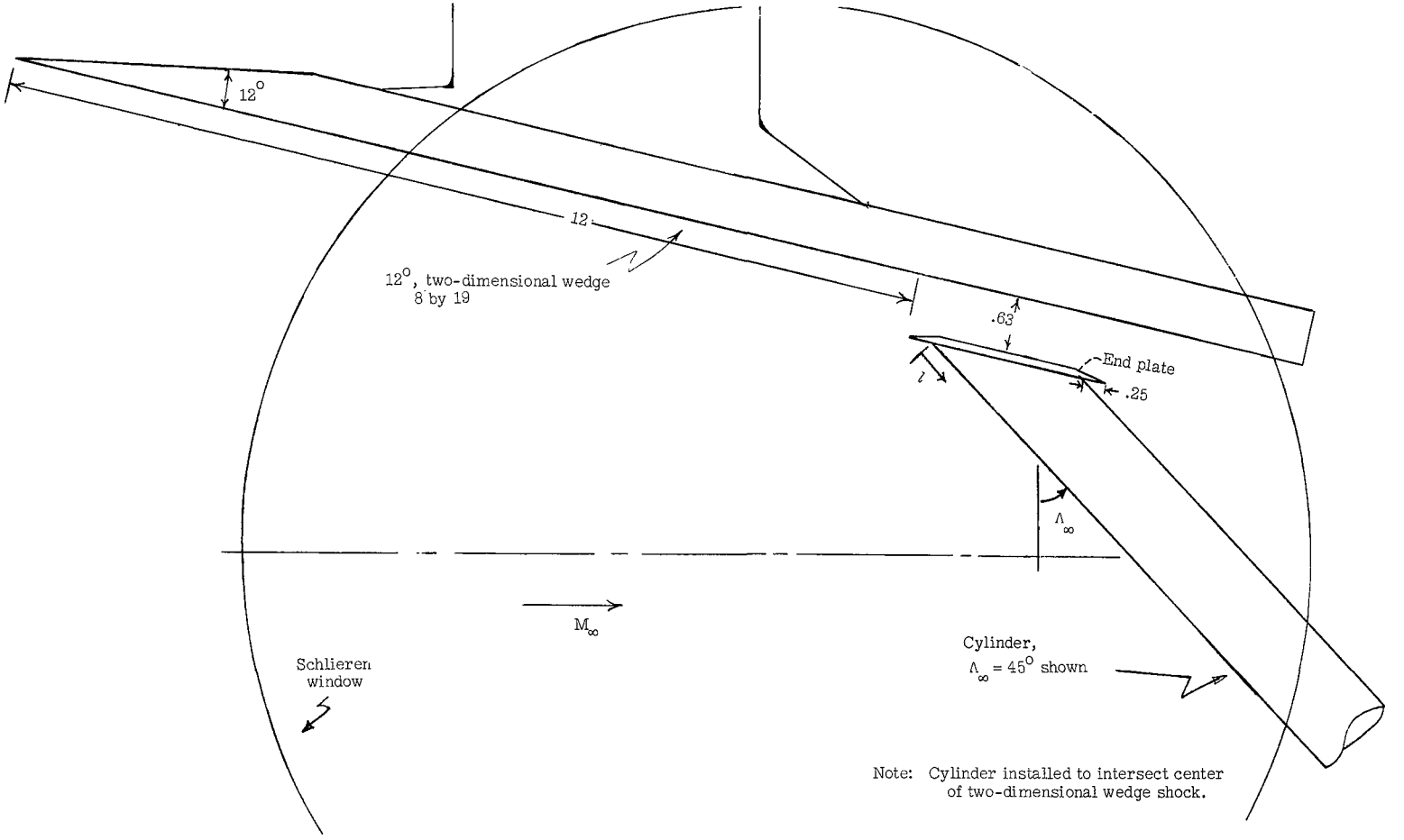

(a) Cylinder and wedge separated.

Figure 1.- Test configurations. All lengths have been nondimensionalized with respect to cylinder diameter D.

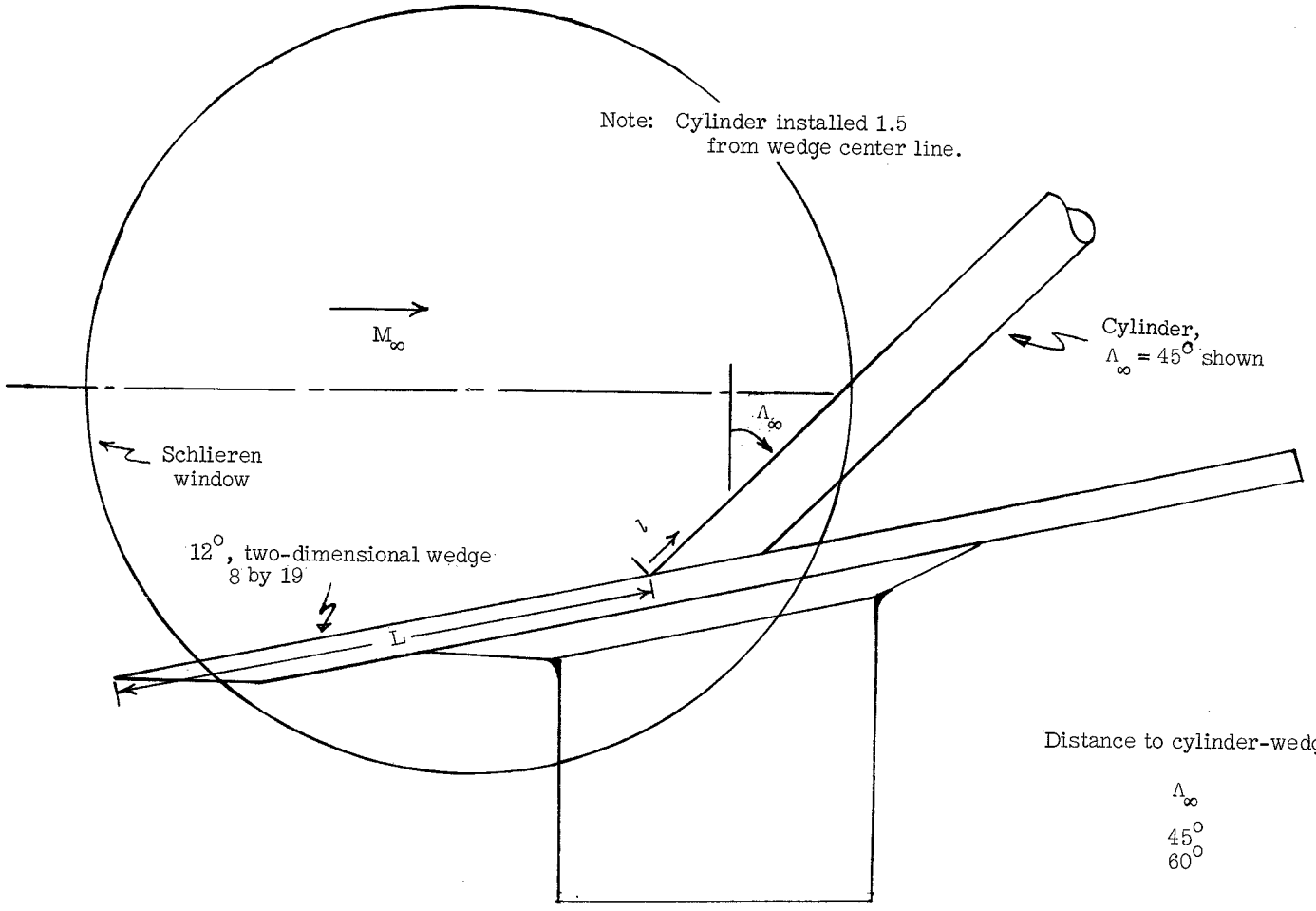

Distance to cylinder-wedge intersection

Λ_∞	L
45°	8.75
60°	7.50

(b) Cylinder and wedge attached.

Figure 1.- Concluded.

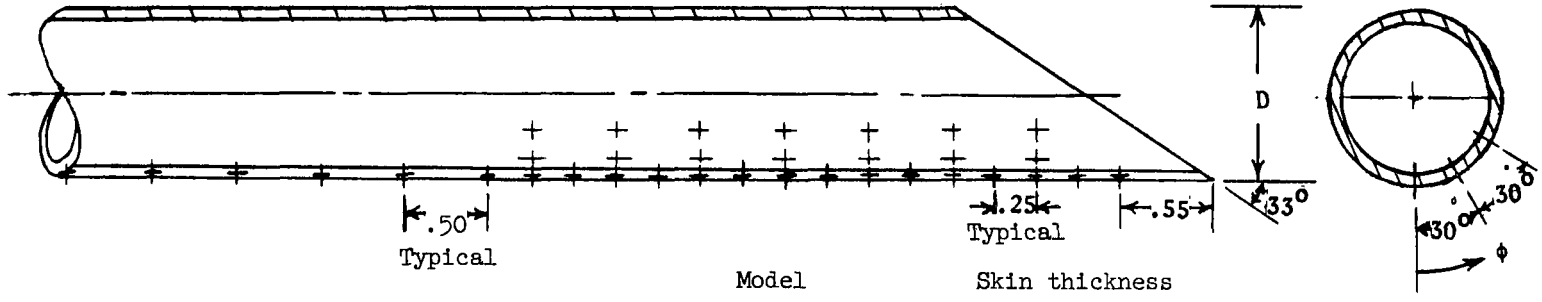

(a) $\Lambda_\infty = 45^0$.

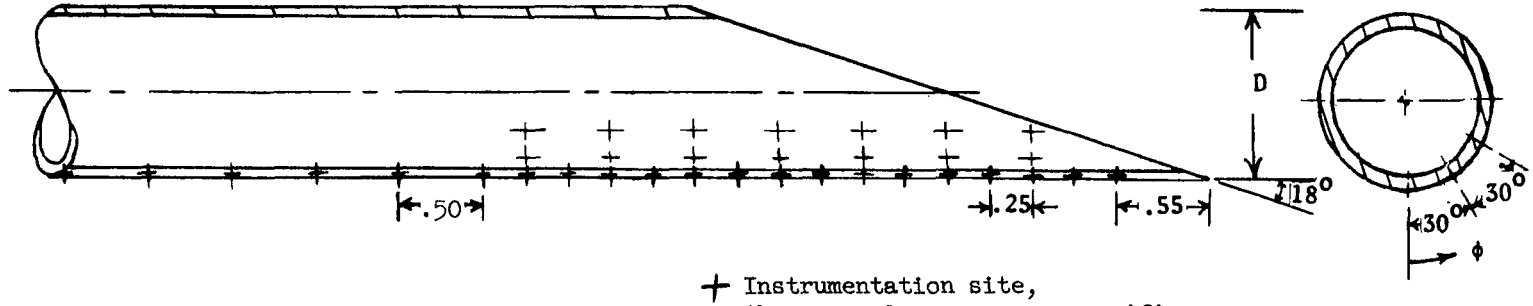

(b) $\Lambda_\infty = 60^0$.

Figure 2.- Sketch of cylinders showing location of heat-transfer and pressure instrumentation. All lengths have been nondimensionalized with respect to cylinder diameter D.

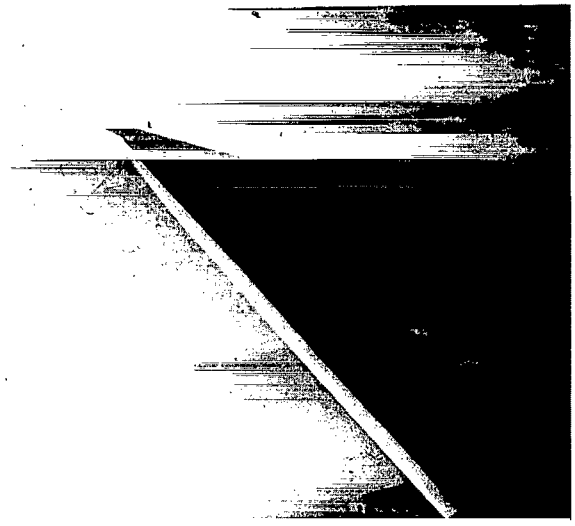

(a) Undisturbed cylinder. $R_{\infty,D} = 3.21 \times 10^5$.

(b) Cylinder and wedge separated. $R_{\infty,D} = 2.28 \times 10^5$; $R_{\omega,D} = 3.27 \times 10^5$.

(c) Cylinder and wedge attached. $R_{\infty,D} = 1.34 \times 10^5$; $R_{\omega,D} = 1.94 \times 10^5$.

L-65-186

Figure 3.- Schlieren photographs for configurations with cylinder swept back 45^0.

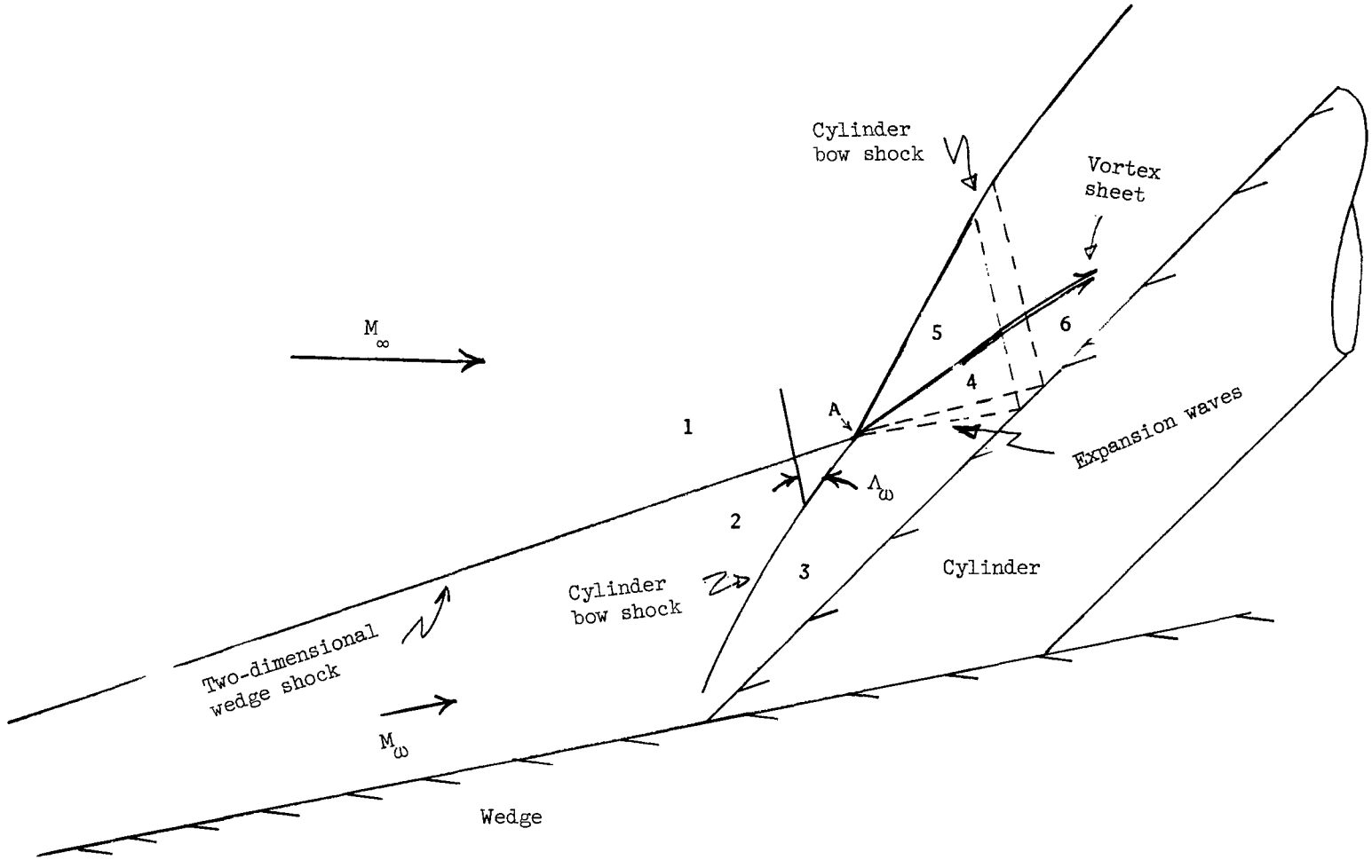

Figure 4.- Schematic sketch of typical schlieren photograph showing inviscid flow-field phenomena associated with intersection of two right running shocks.

(a) Undisturbed cylinder. $R_{\infty,D} = 3.32 \times 10^5$.

(b) Cylinder and wedge separated. $R_{\infty,D} = 1.47 \times 10^5$; $R_{\omega,D} = 2.1 \times 10^5$.

L-65-187

(c) Cylinder and wedge attached. $R_{\infty,D} = 1.47 \times 10^5$; $R_{\omega,D} = 2.1 \times 10^5$.

Figure 5.- Schlieren photographs of configurations with cylinder swept back 60^0.

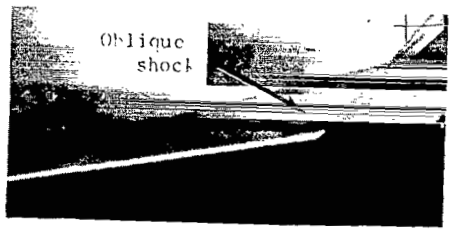

(a) $R_{\infty,D} = 0.94 \times 10^5$; $R_{\omega,D} = 1.34 \times 10^5$.

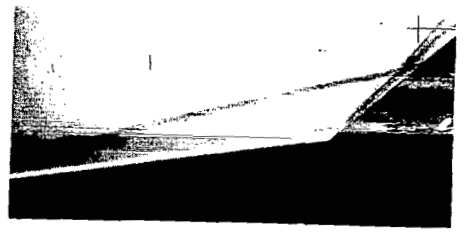

(b) $R_{\infty,D} = 1.34 \times 10^5$; $R_{\omega,D} = 1.94 \times 10^5$.

(c) $R_{\infty,D} = 1.73 \times 10^5$; $R_{\omega,D} = 2.5 \times 10^5$.

(d) $R_{\infty,D} = 2.13 \times 10^5$; $R_{\omega,D} = 3.0 \times 10^5$.

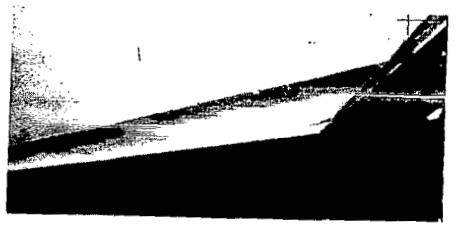

(e) $R_{\infty,D} = 2.5 \times 10^5$; $R_{\omega,D} = 3.6 \times 10^5$.

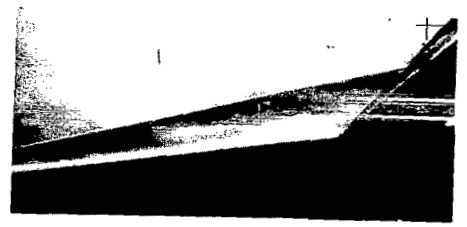

(f) $R_{\infty,D} = 2.66 \times 10^5$; $R_{\omega,D} = 3.83 \times 10^5$.

(g) $R_{\infty,D} = 3.05 \times 10^5$; $R_{\omega,D} = 4.55 \times 10^5$.

L-65-188

(h) $R_{\infty,D} = 3.51 \times 10^5$; $R_{\omega,D} = 5.01 \times 10^5$.

Figure 6.- Schlieren photographs for $\Lambda_\infty = 45^0$, wedge and cylinder attached, showing extent of root flow separation as a function of Reynolds number. $\frac{T_\omega}{T_0} \approx 0.4$.

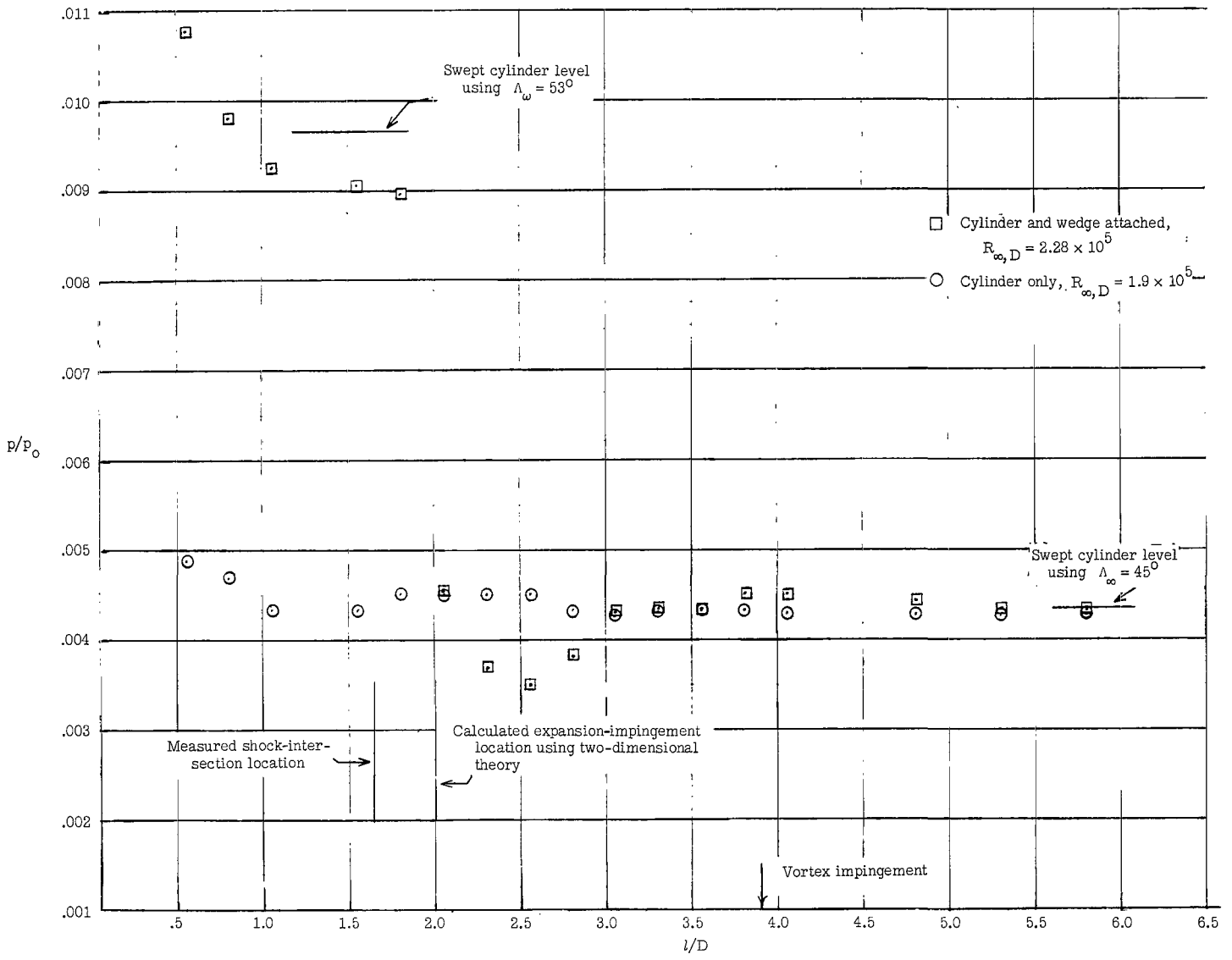

(a) Wedge and cylinder attached compared to undisturbed cylinder.

Figure 7.- Pressure distribution along stagnation line of cylindrical probe. $\Lambda_\infty = 45^0$.

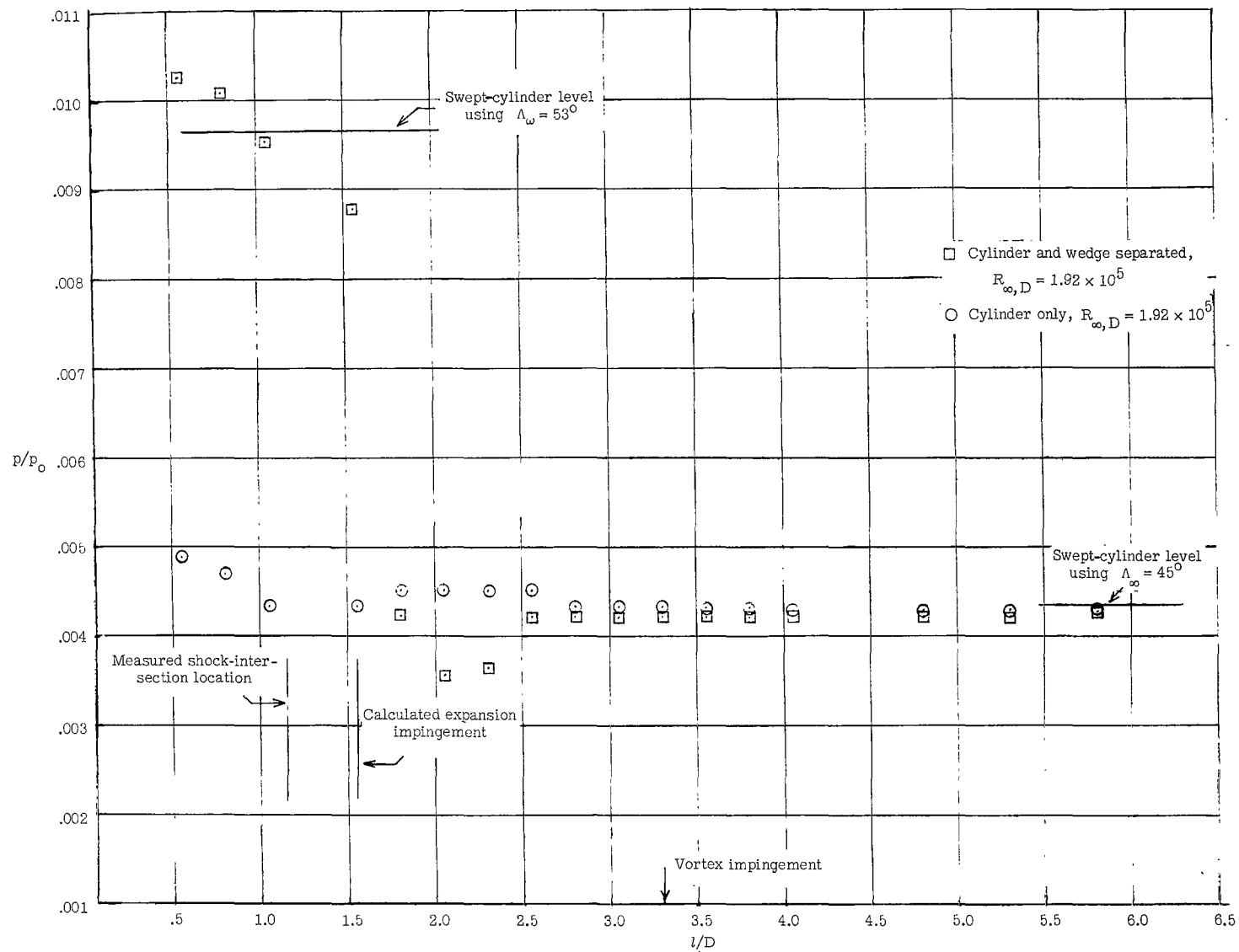

(b) Wedge and cylinder separated compared with undisturbed cylinder.

Figure 7.- Concluded.

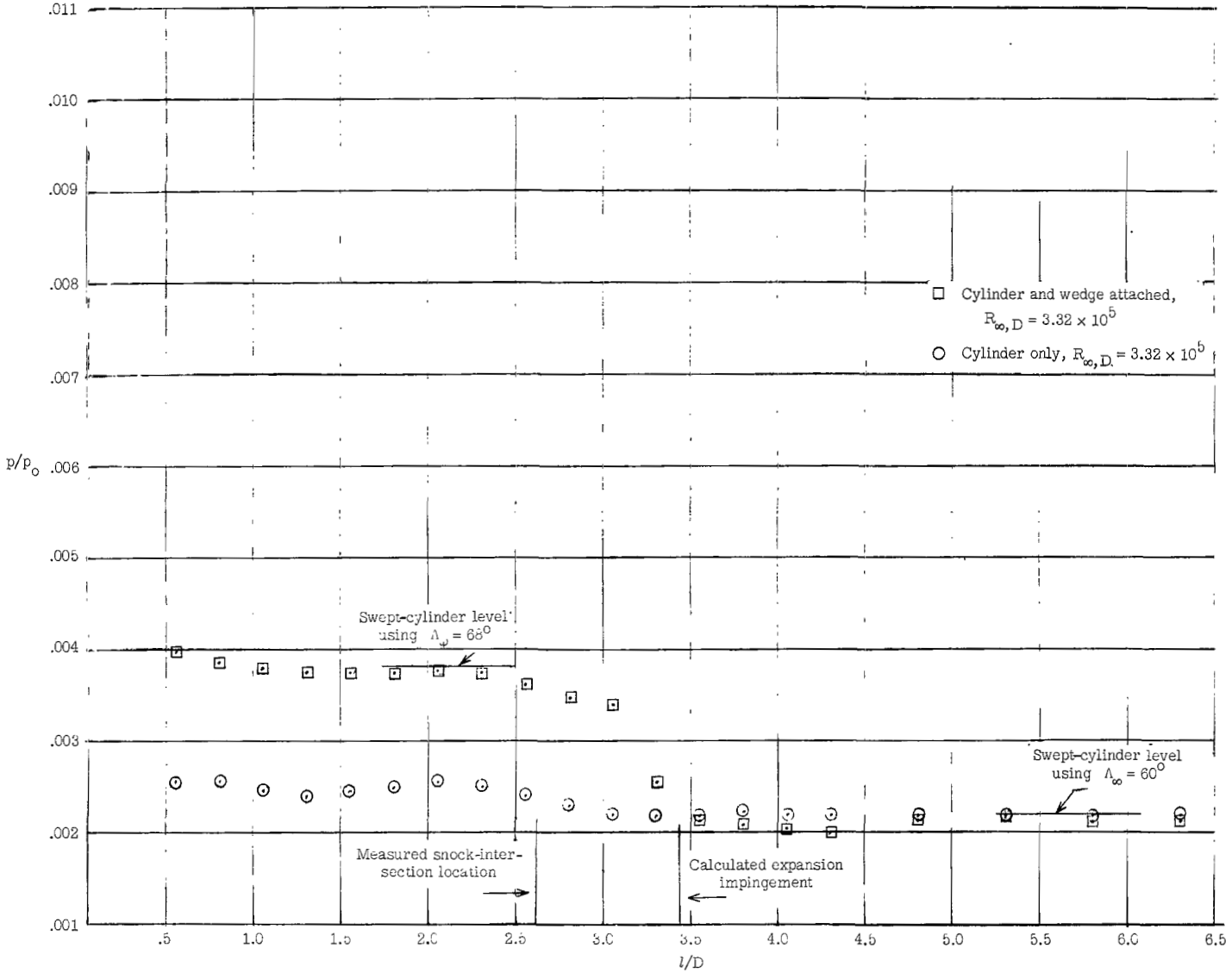

(a) Wedge and cylinder attached compared with undisturbed cylinder.

Figure 8.- Pressure distribution along cylinder stagnation line $\Lambda_\infty = 60^\circ$.

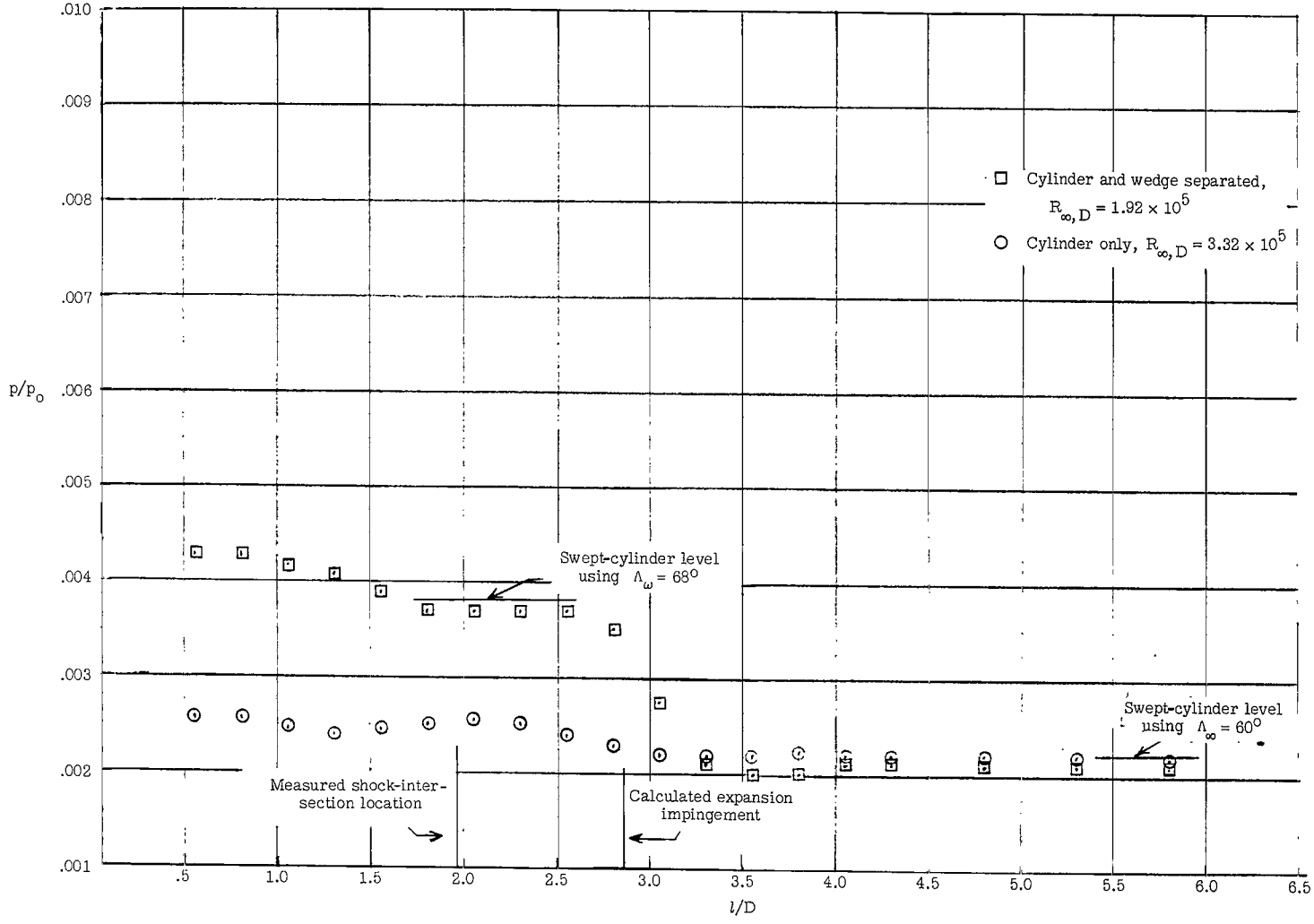

(b) Wedge and cylinder separated compared with undisturbed cylinder.

Figure 8.- Concluded.

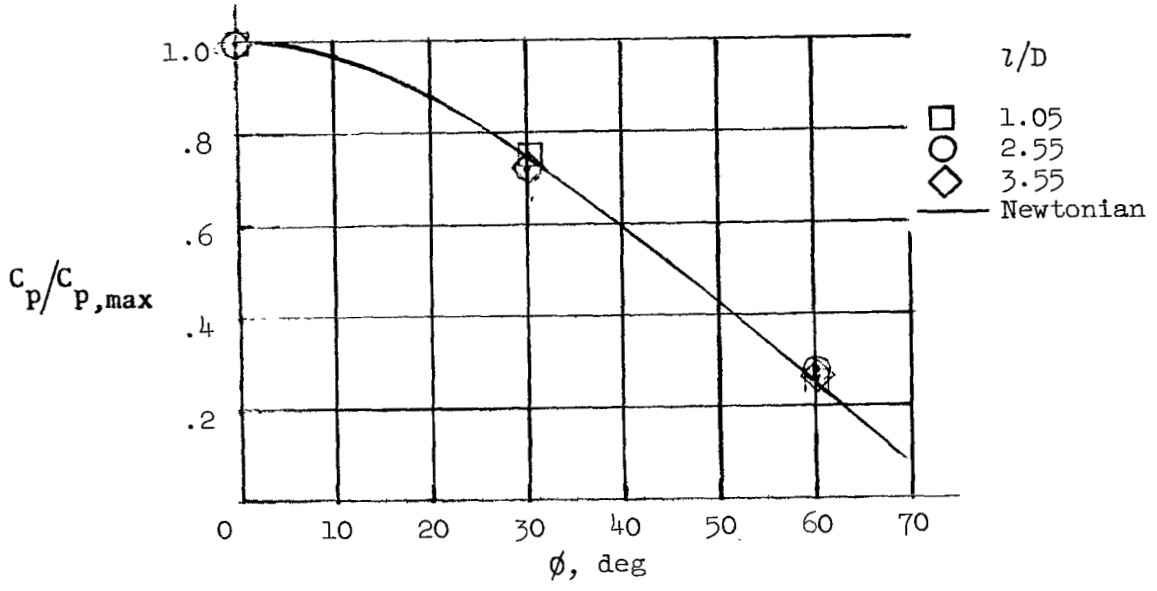

(a) $\Lambda_\infty = 45^0$; $R_{\infty,D} = 1.92 \times 10^5$.

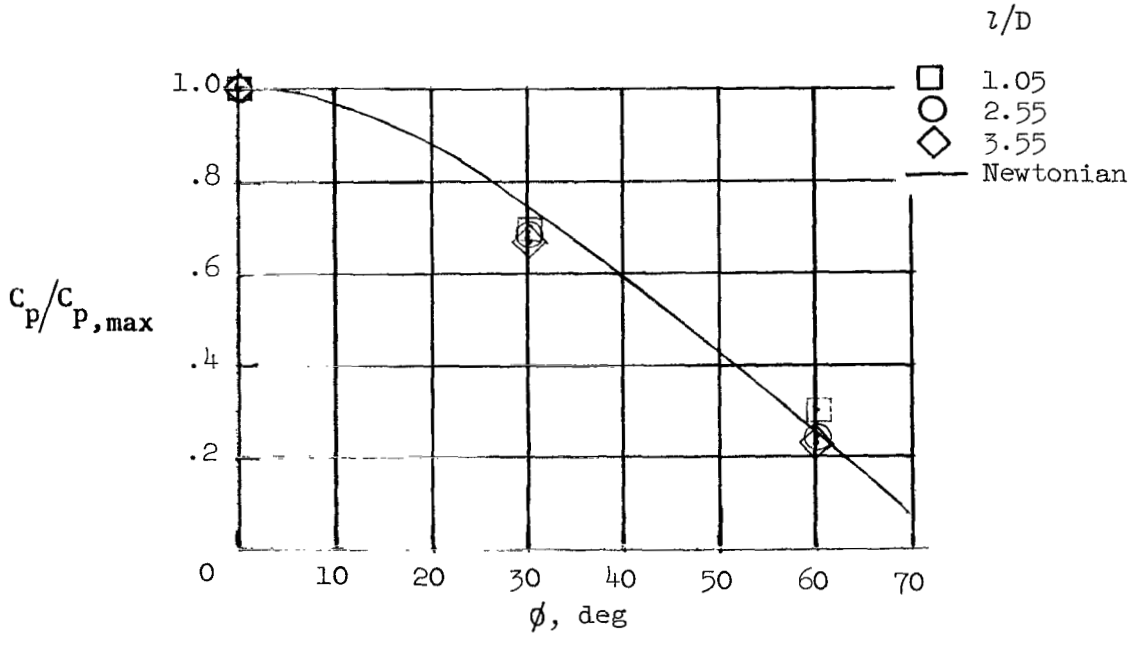

(b) $\Lambda_\infty = 60^0$; $R_{\infty,D} = 3.32 \times 10^5$.

Figure 9.- Chordwise pressure distribution, cylinder only.

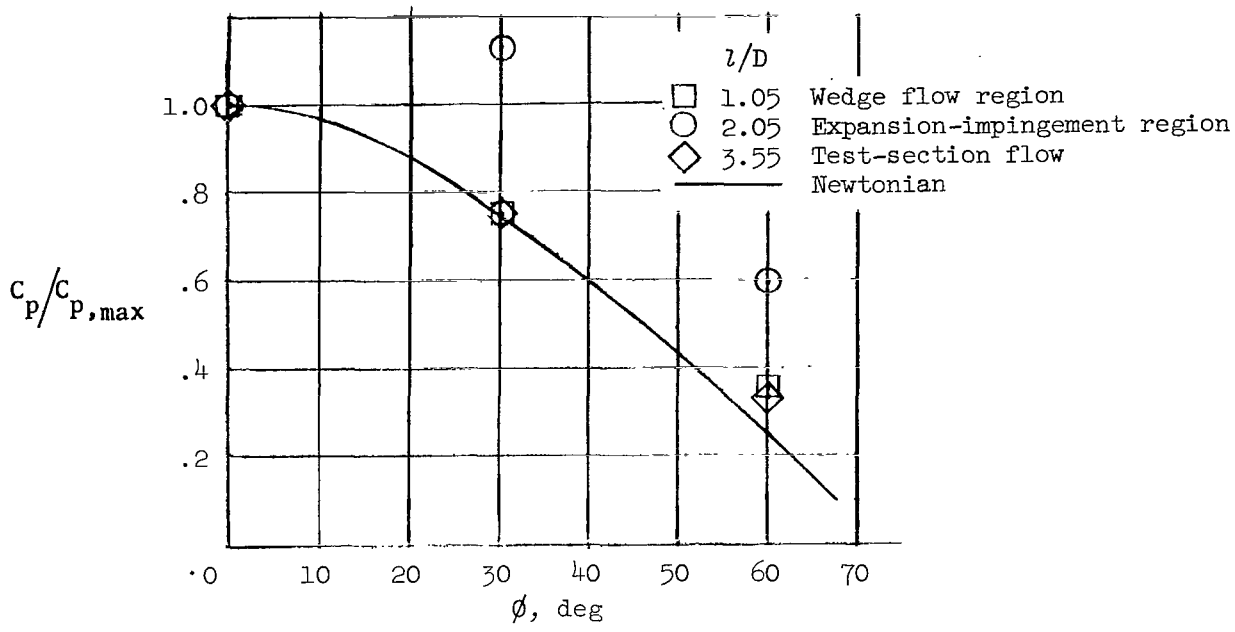

(a) Cylinder and wedge attached. $R_{\infty,D} = 2.28 \times 10^5$.

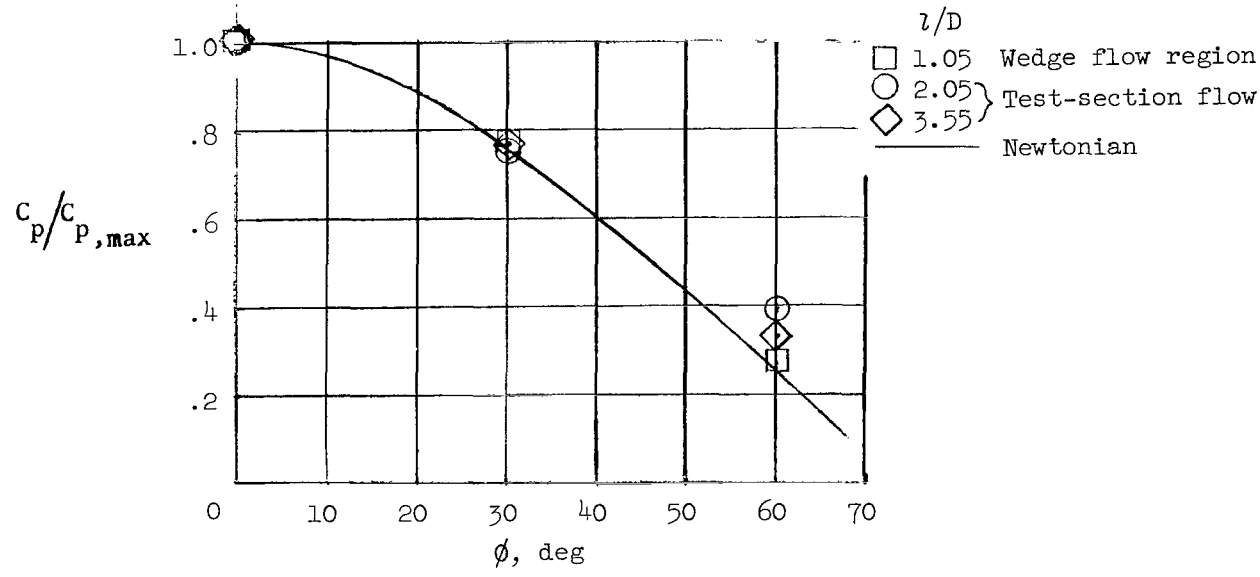

(b) Cylinder and wedge separated. $R_{\infty,D} = 1.92 \times 10^5$.

Figure 10.- Chordwise pressure distribution. $\Lambda_\infty = 45^0$.

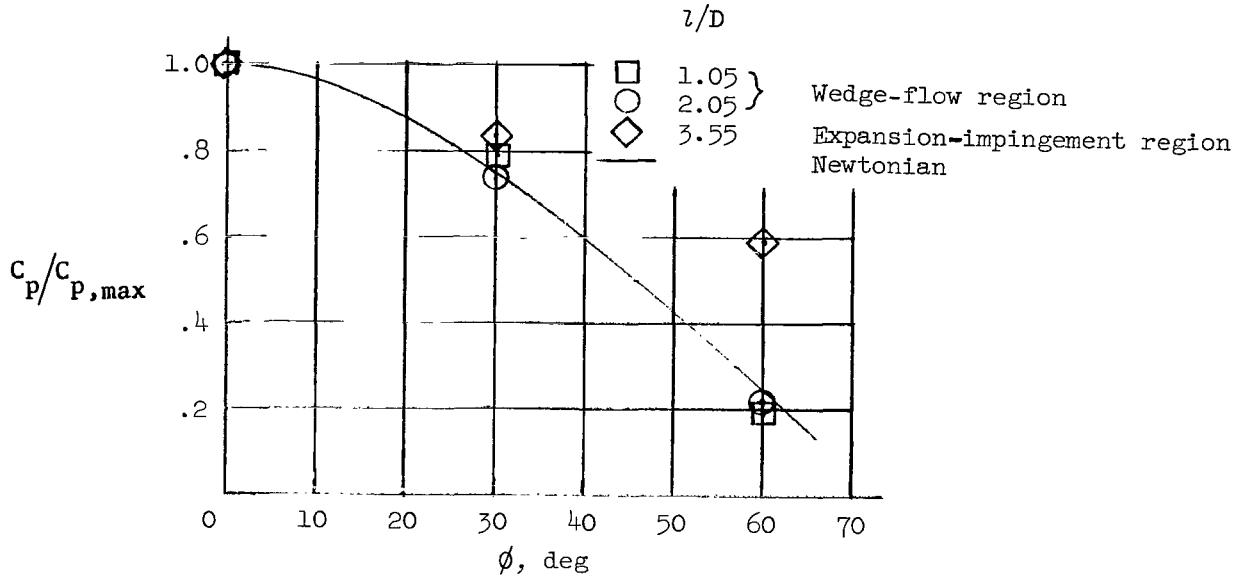

(a) Cylinder and wedge attached. $R_{\infty,D} = 3.32 \times 10^5$.

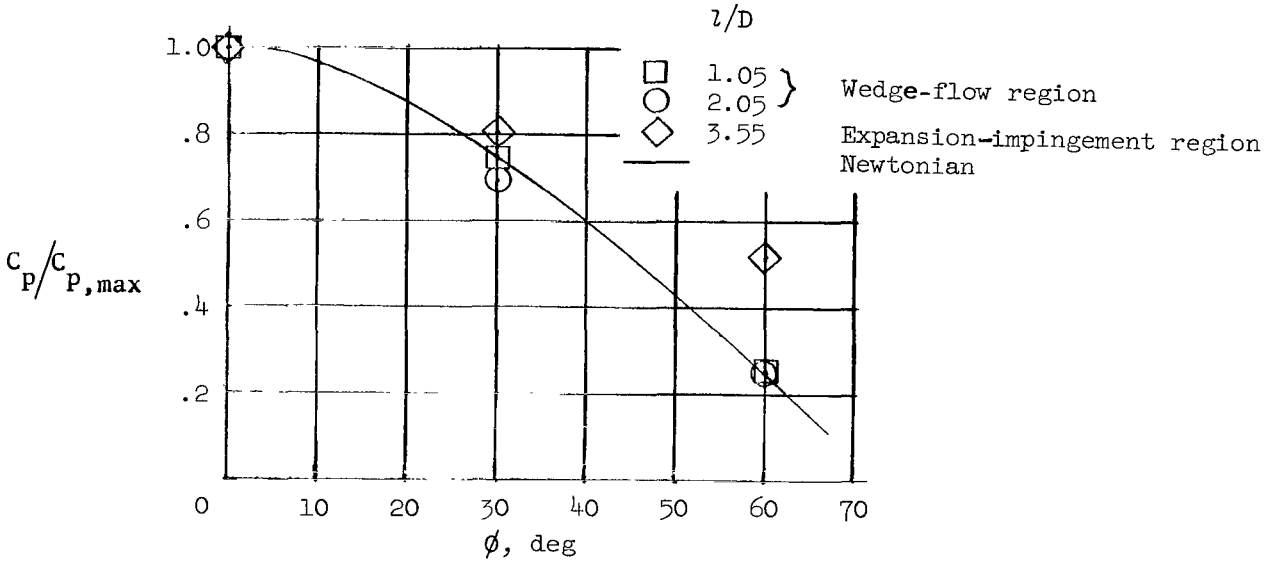

(b) Cylinder and wedge separated. $R_{\infty,D} = 3.32 \times 10^5$.

Figure 11.- Chordwise pressure distribution. $\Lambda_\infty = 60^0$.

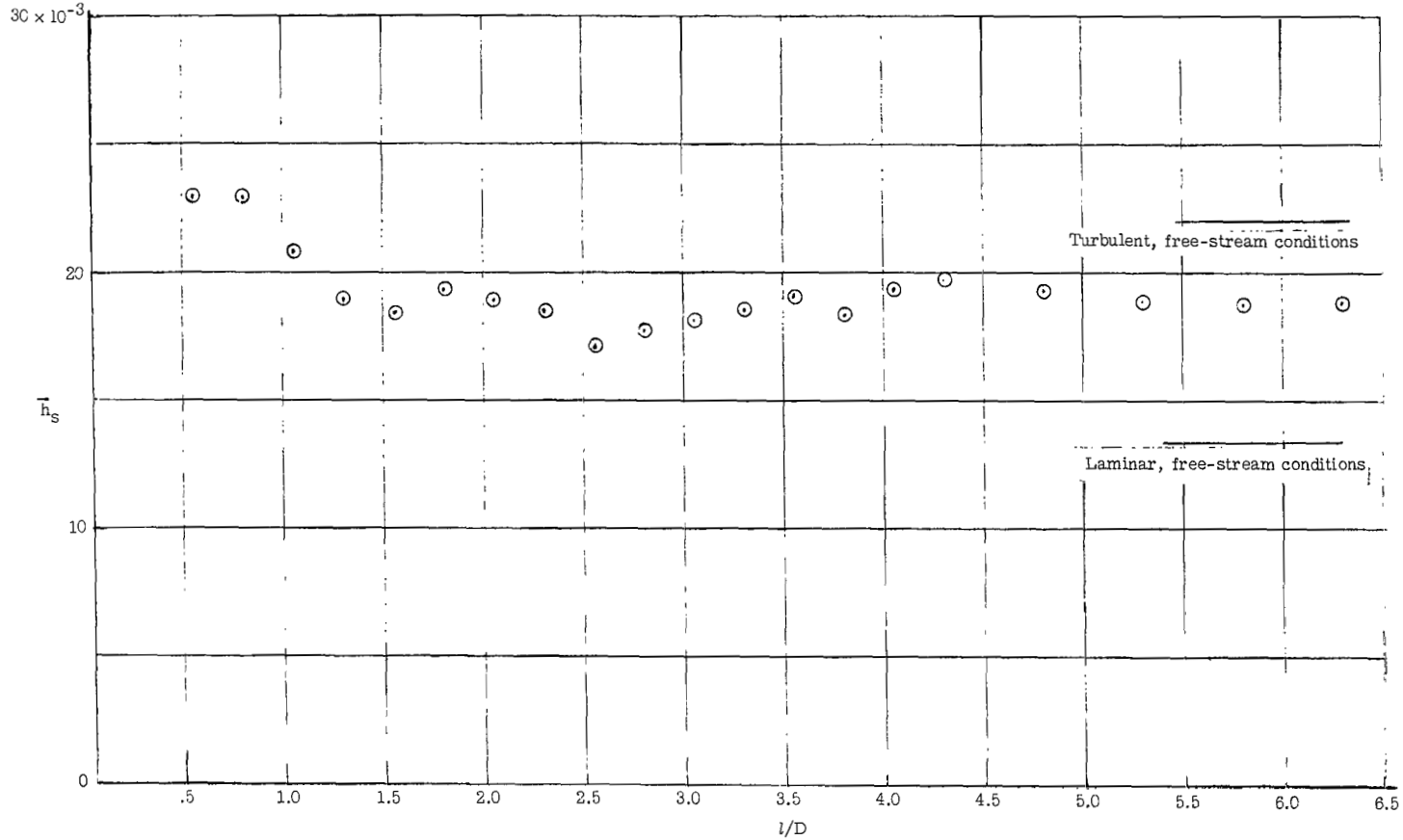

(a) $\Lambda_\infty = 45^0$.

Figure 12.- Heat-transfer-coefficient distribution along cylinder stagnation line for undisturbed cylinder. $R_{\infty,D} = 2.55 \times 10^5$.

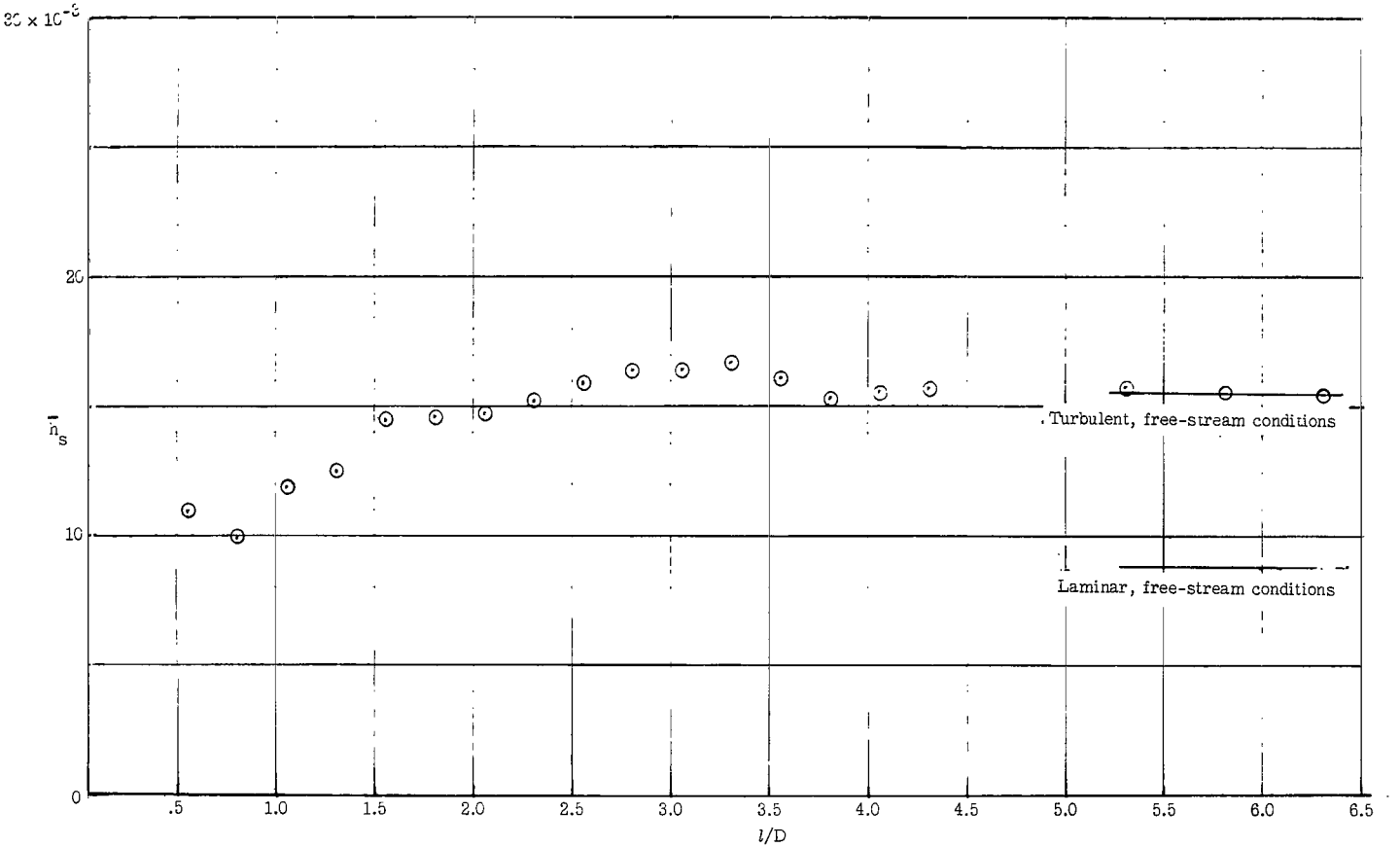

(b) $\Lambda_\infty = 60^0$.

Figure 12.- Concluded.

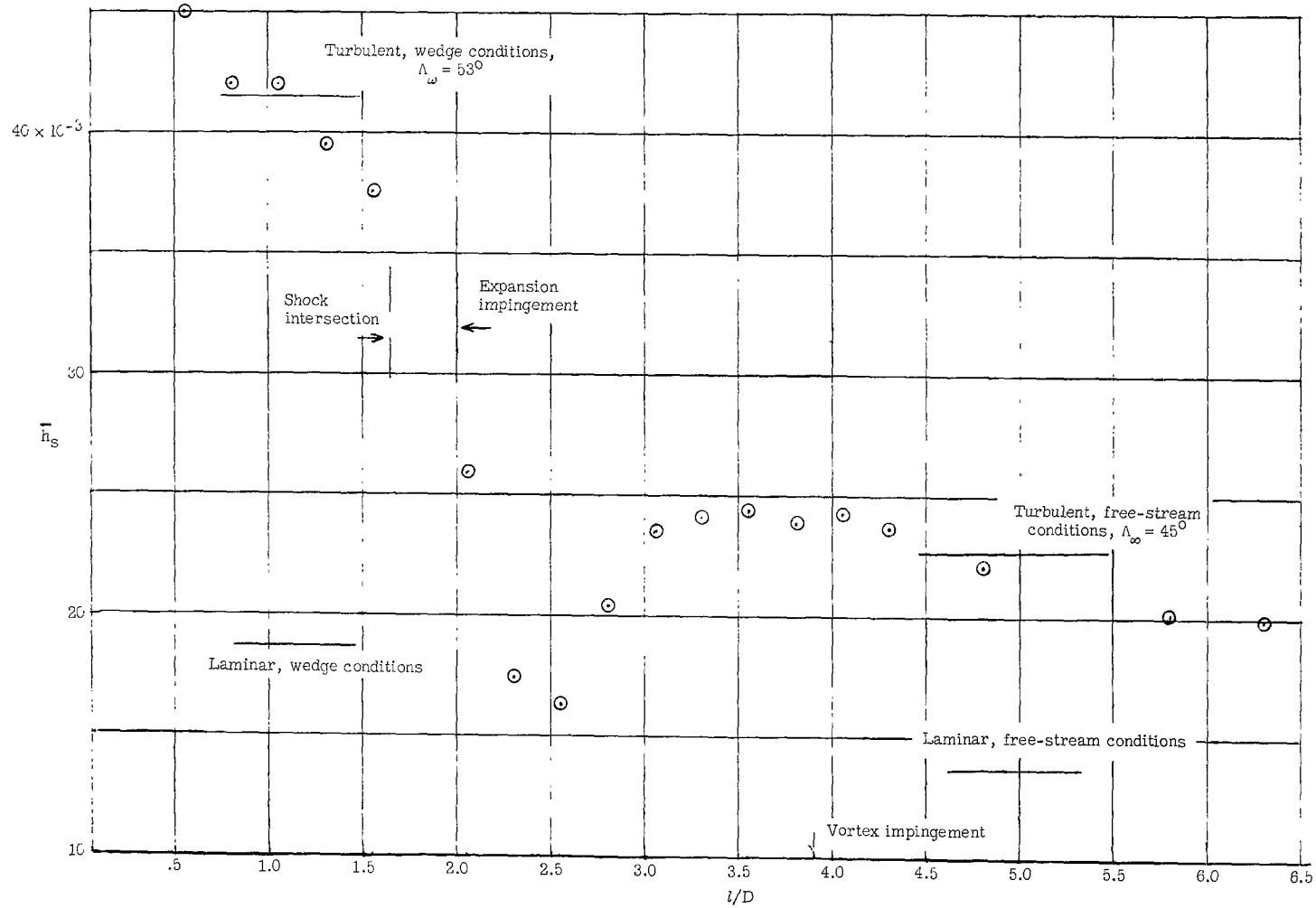

(a) Wedge and cylinder attached. $R_{\infty,D} = 2.66 \times 10^5$; $R_{\omega,D} = 3.83 \times 10^5$.

Figure 13.- Heat-transfer-coefficient distribution along cylinder stagnation line. $\Lambda_\infty = 45^\circ$; $\Lambda_\omega = 53^\circ$.

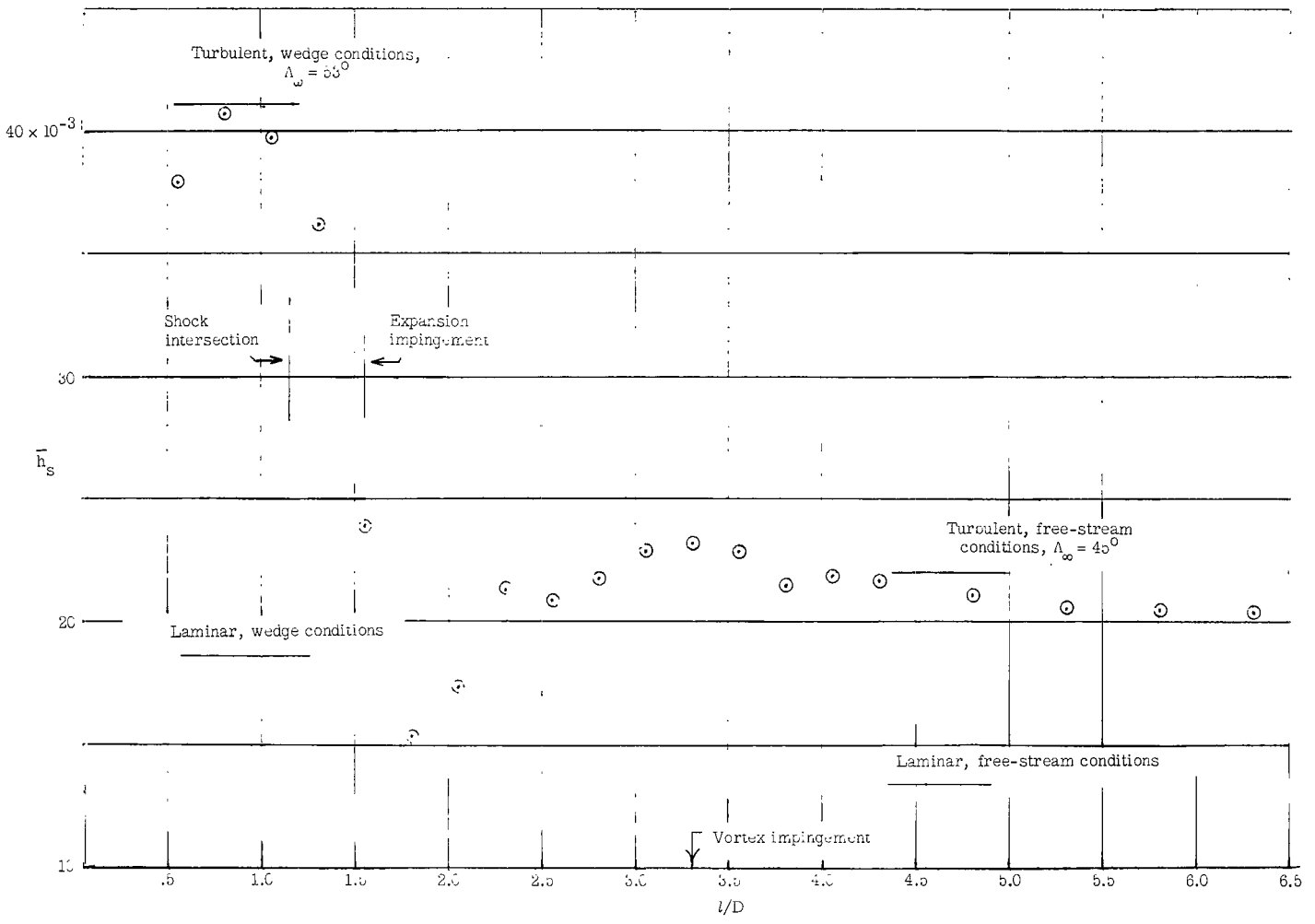

(b) Wedge and cylinder separated. $R_{\infty,D} = 2.54 \times 10^5$; $R_{\omega,D} = 3.77 \times 10^5$.

Figure 13.- Continued.

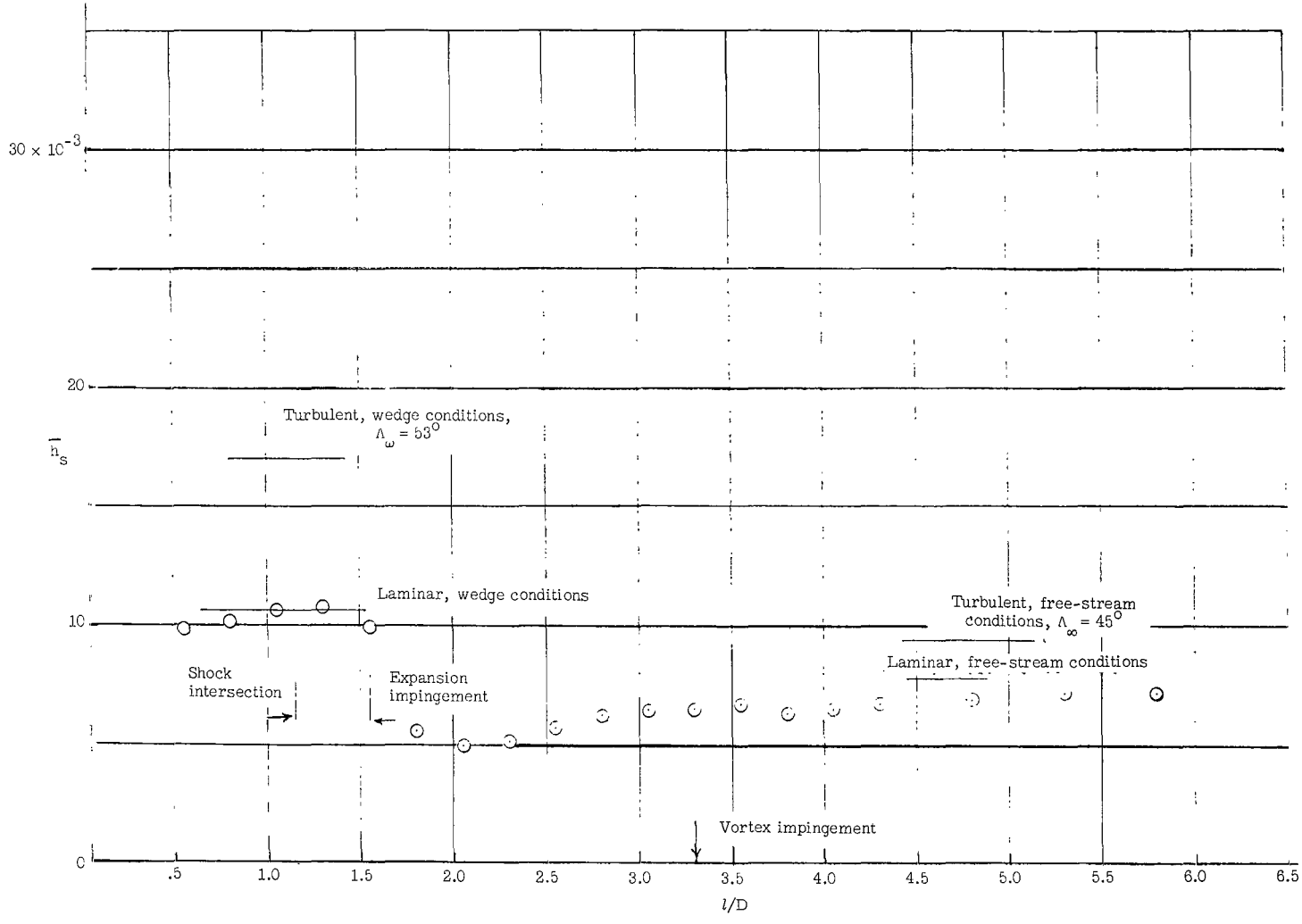

(c) Wedge and cylinder separated. $R_{\infty,D} = 0.87 \times 10^5$; $R_{\omega,D} = 1.26 \times 10^5$.

Figure 13.- Concluded.

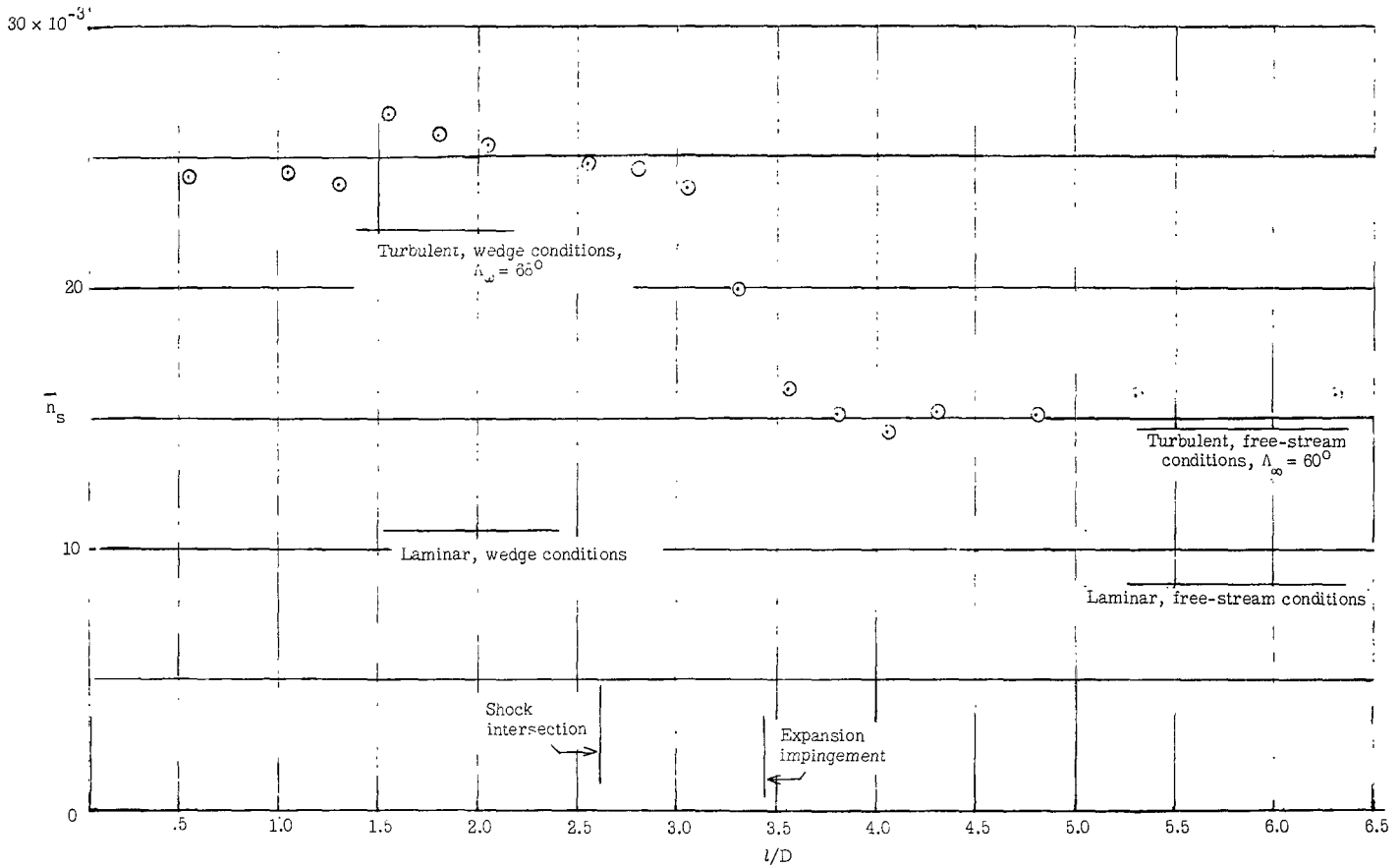

(a) Wedge and cylinder attached. $R_{\infty,D} = 2.46 \times 10^5$; $R_{\omega,D} = 3.5 \times 10^5$.

Figure 14.- Heat-transfer-coefficient distribution along cylinder stagnation line. $\Lambda_\infty = 60^\circ$; $\Lambda_\omega = 68^\circ$.

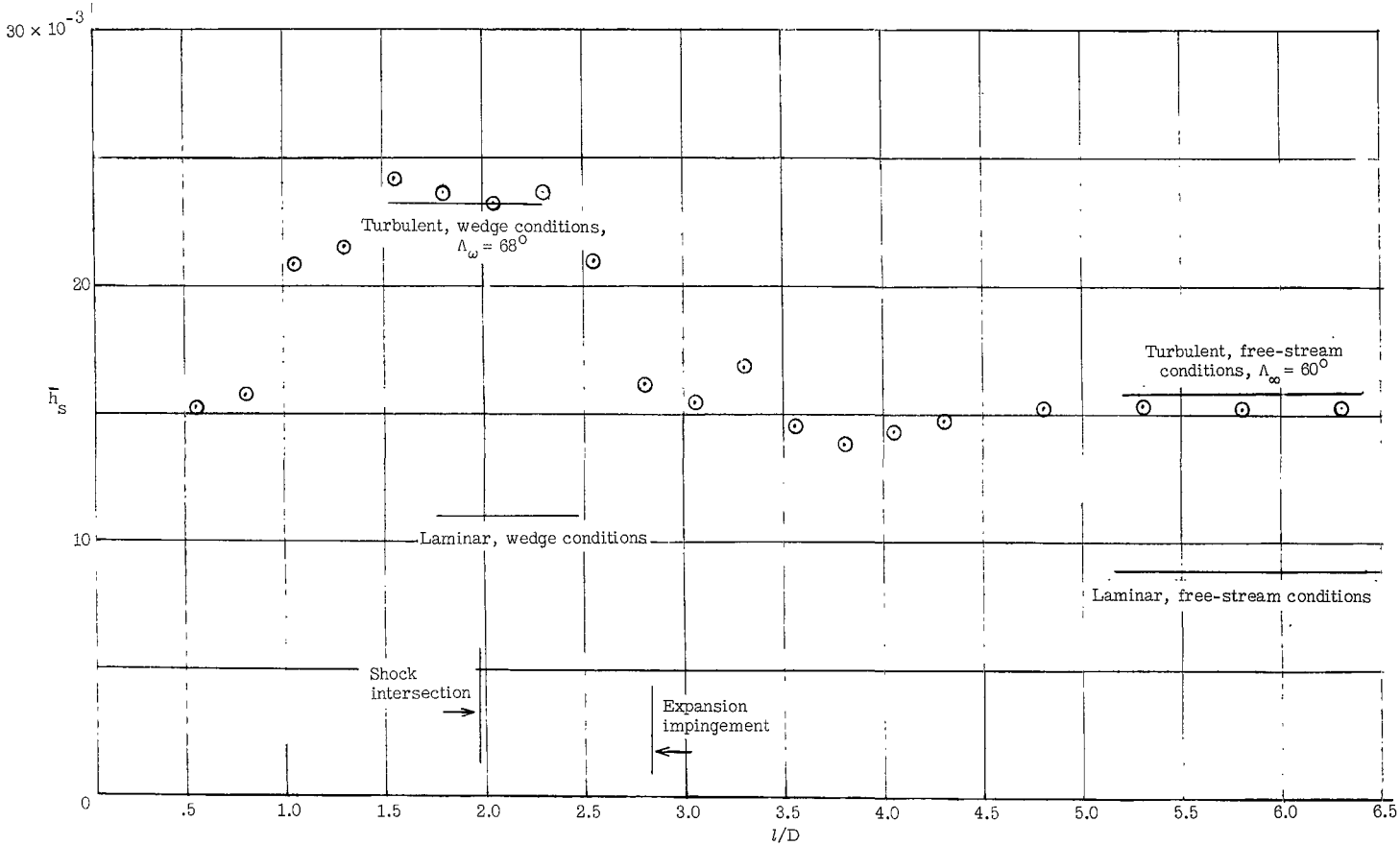

(b) Wedge and cylinder separated. $R_{\infty,D} = 2.58 \times 10^5$; $R_{\omega,D} = 3.7 \times 10^5$.

Figure 14.- Continued.

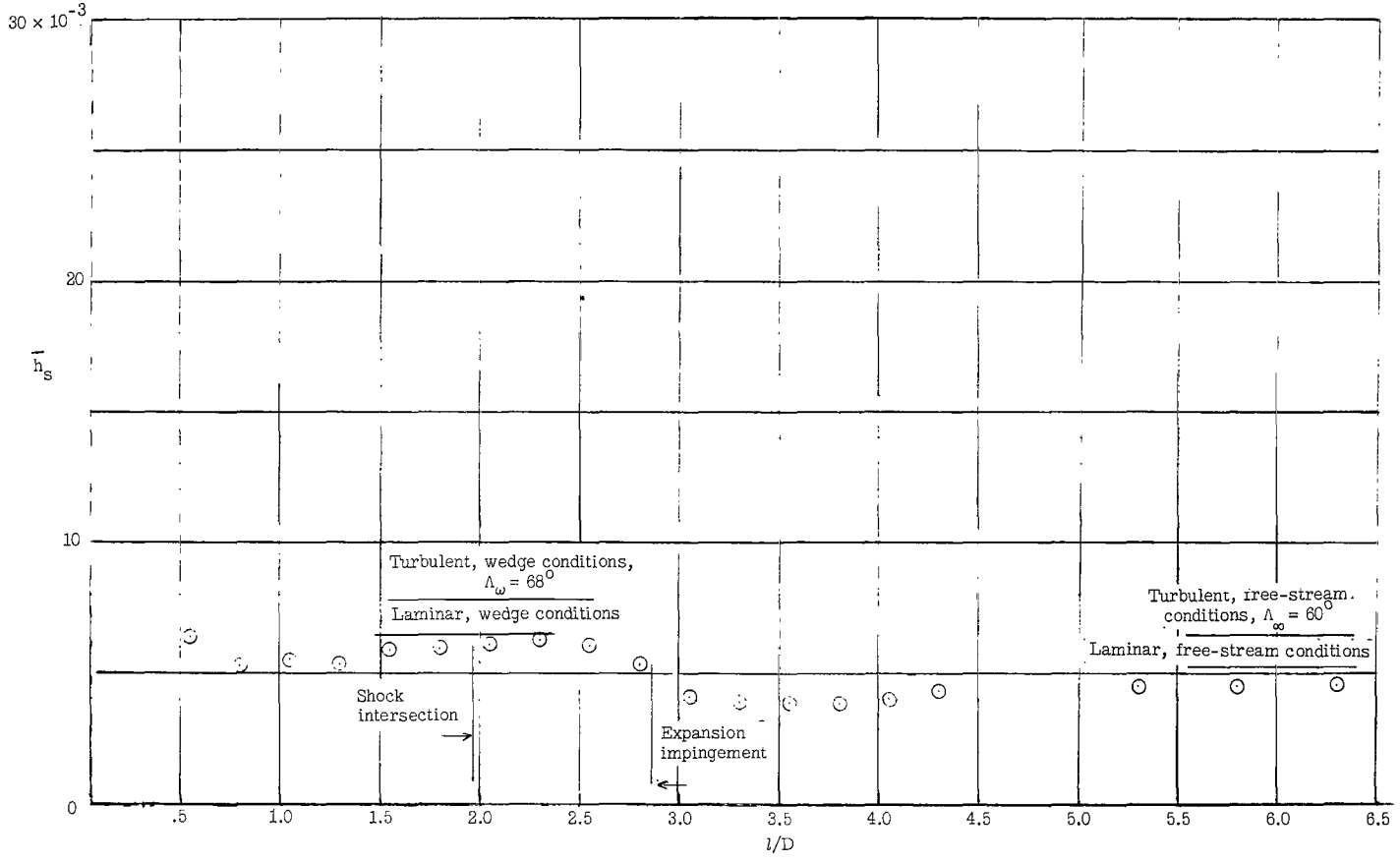

(c) Wedge and cylinder separated. $R_{\infty,D} = 0.89 \times 10^5$; $R_{\omega,D} = 1.28 \times 10^5$.

Figure 14.- Concluded.

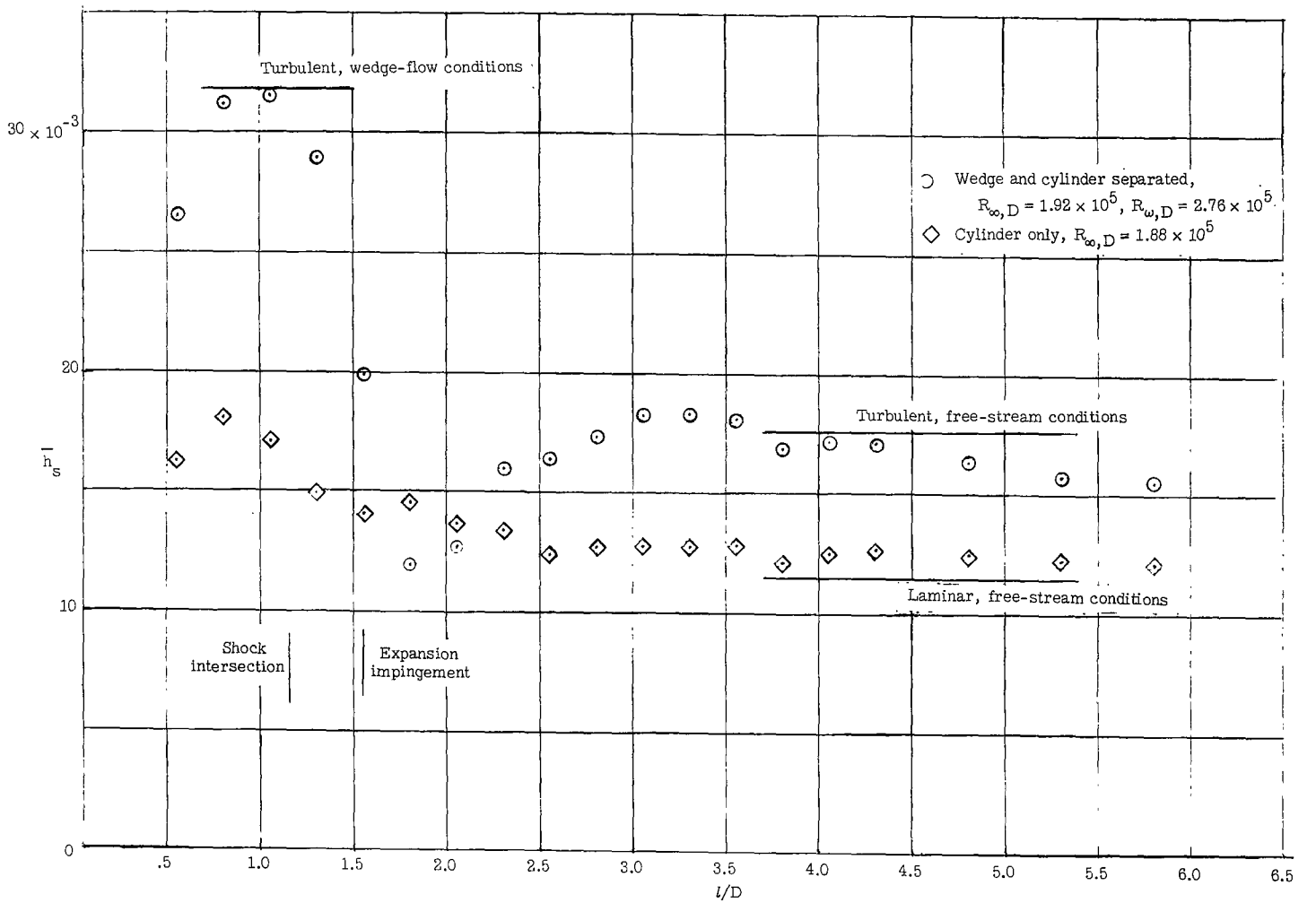

Figure 15.- Heat-transfer-coefficient distribution along cylinder stagnation line showing effect of wedge flow field on state of stagnation-line boundary layer in undisturbed region. $\Lambda_\infty = 45^0$.

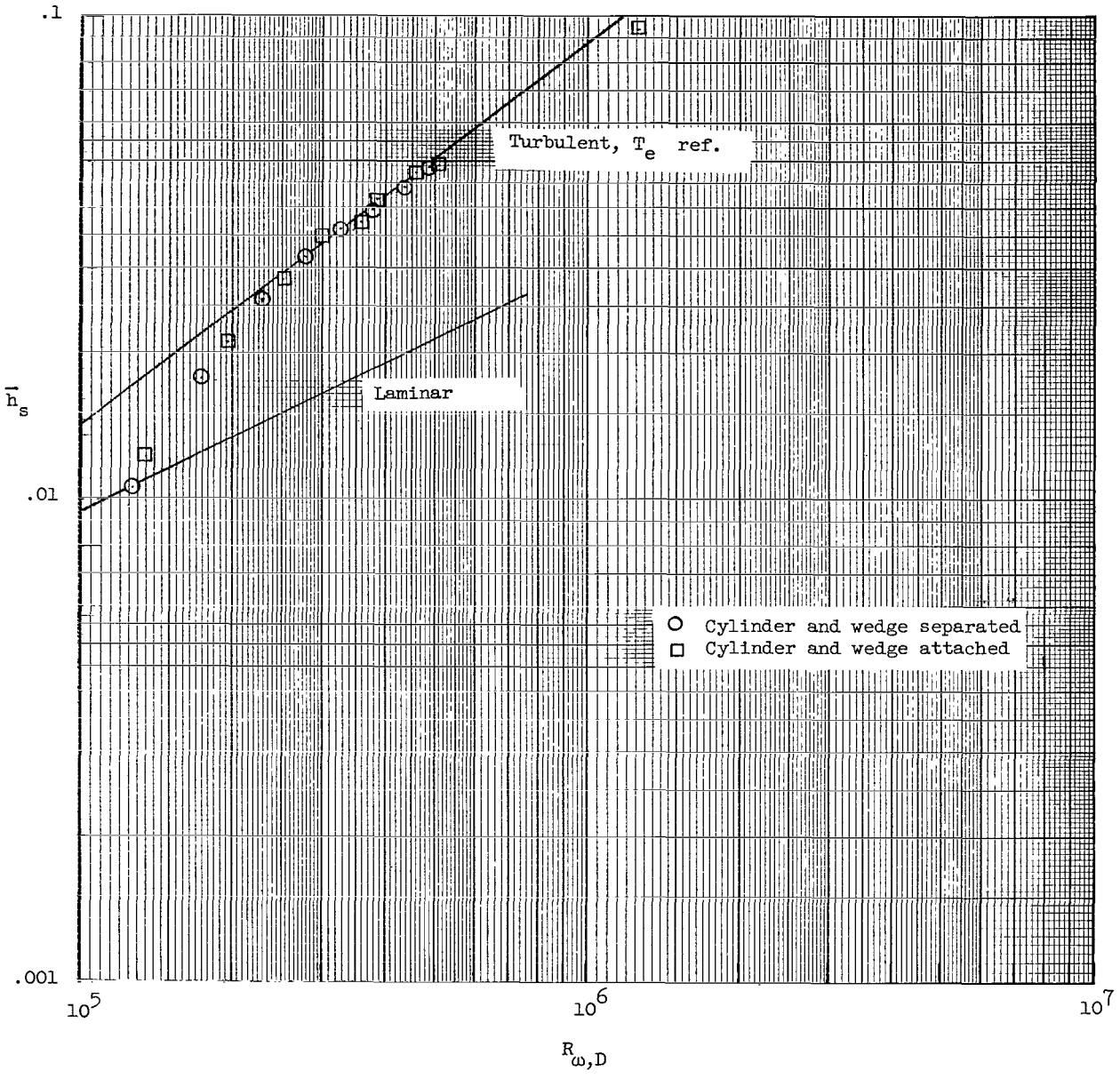

(a) Wedge flow region. $l/D = 1.05$; $\Lambda_\omega = 53^0$; $M_\omega = 5.3$; $T_0 \approx 1360^0$ R.

Figure 16.- Stagnation-line heat-transfer coefficient as a function of unit Reynolds number. $\Lambda_\infty = 45^0$.

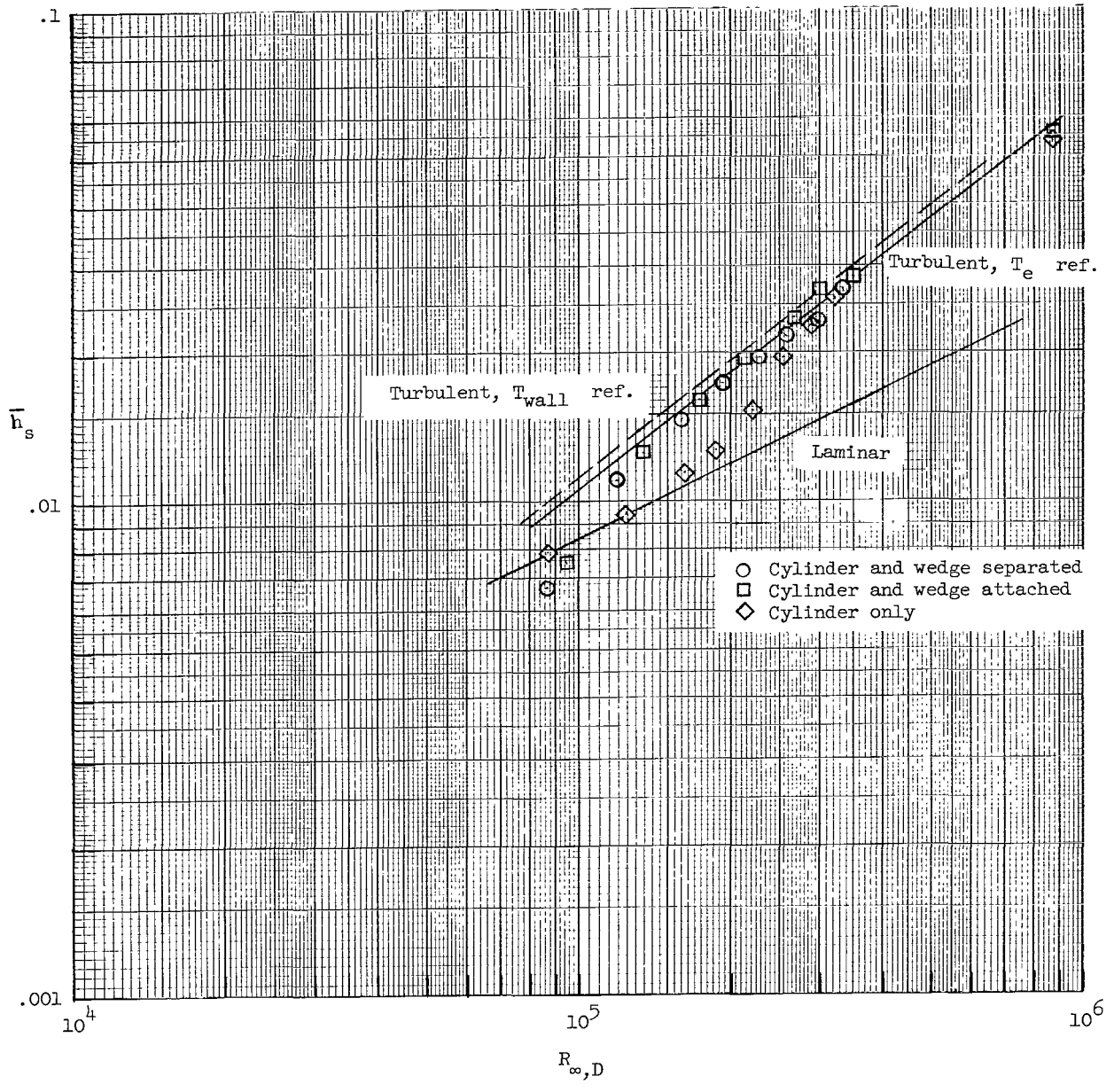

(b) Undisturbed flow region. $l/D = 4.3$; $M_\infty = 7.95$; $\Lambda_\infty = 45^0$; $T_0 \approx 1325^0$ R.

Figure 16.- Concluded.

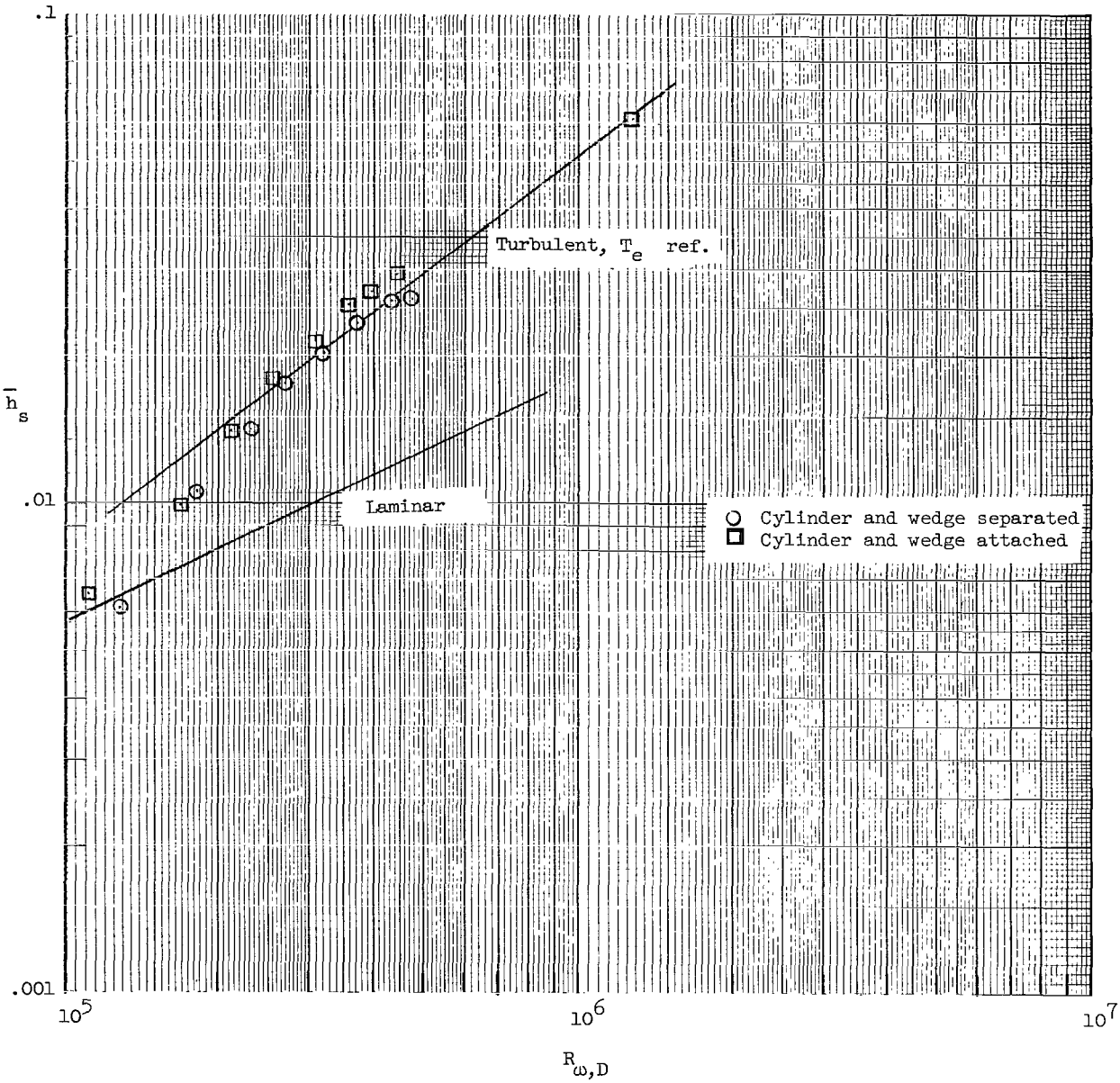

(a) Wedge flow region. $l/D = 2.05$; $\Lambda_\omega = 68^o$; $M_\omega = 5.3$; $T_0 \approx 1450^o$ R.

Figure 17.- Stagnation-line heat-transfer coefficient as a function of unit Reynolds number. $\Lambda_\infty = 60^o$.

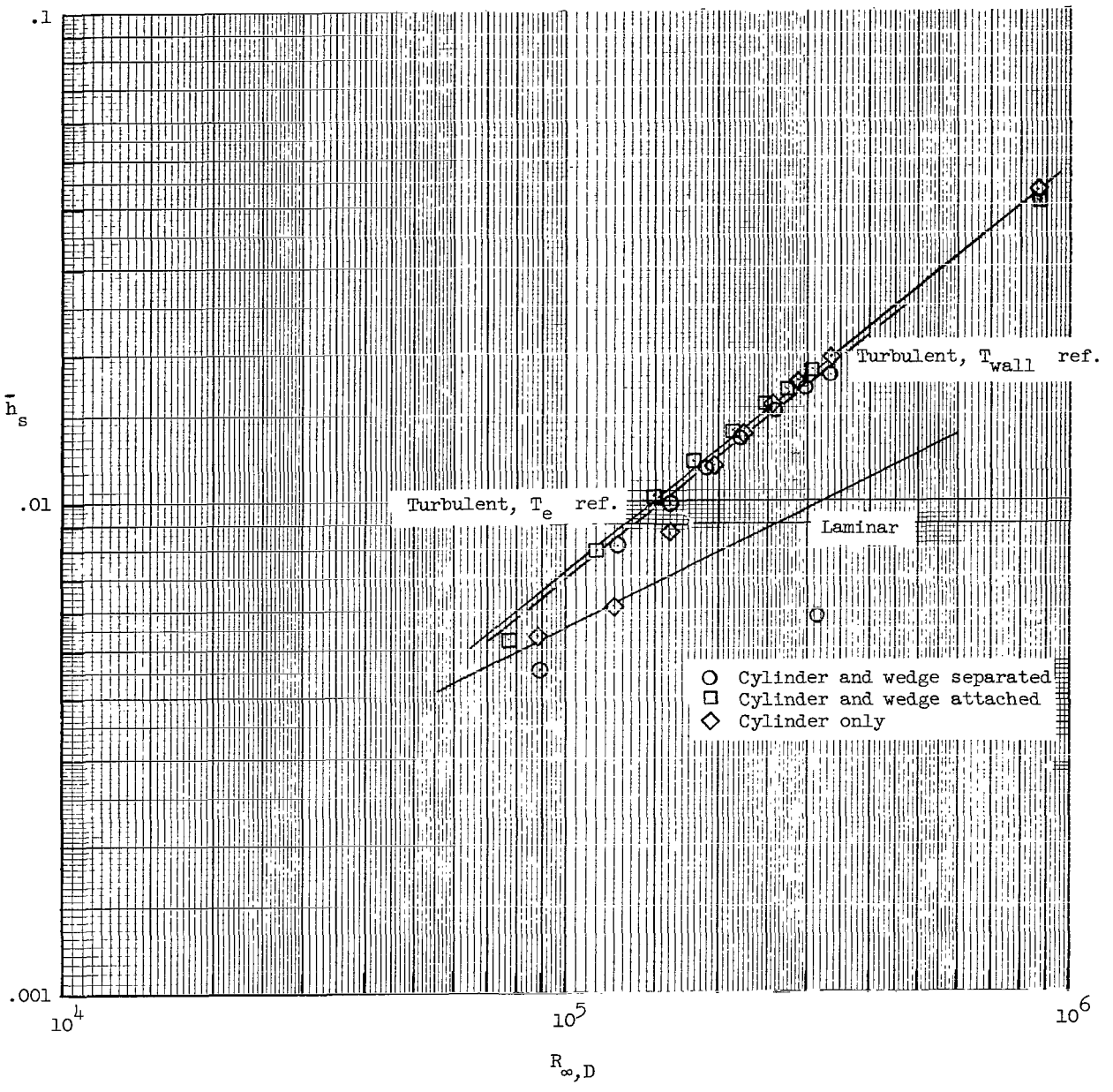

(b) Undisturbed flow region. $l/D = 5.3$; $\Lambda_\infty = 60^0$; $M_\infty = 7.95$; $T_0 \approx 1330^0$ R.

Figure 17.- Concluded.

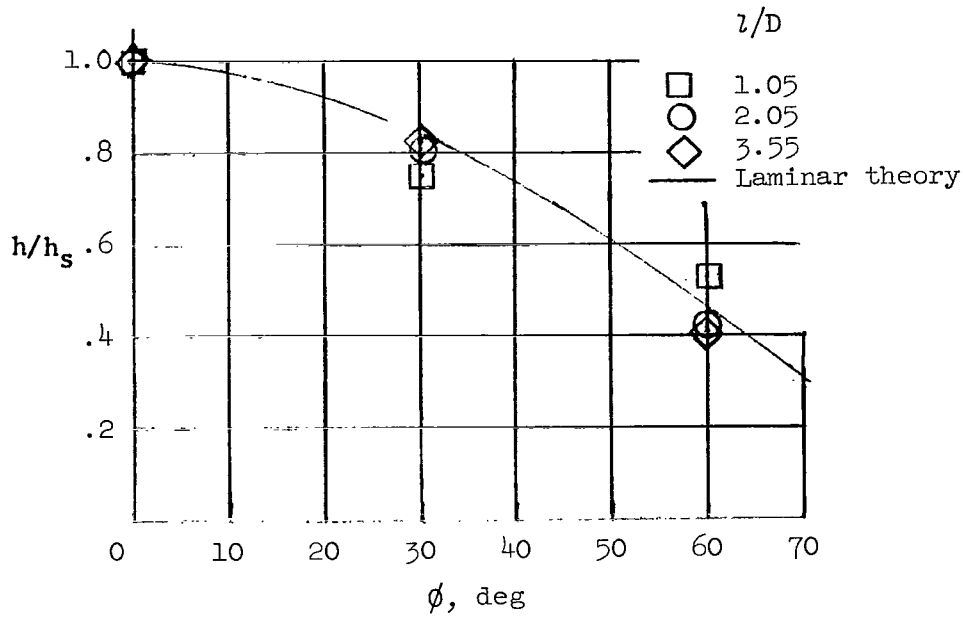

(a) $R_{\infty,D} = 1.25 \times 10^5$; $\Lambda_\infty = 60^0$.

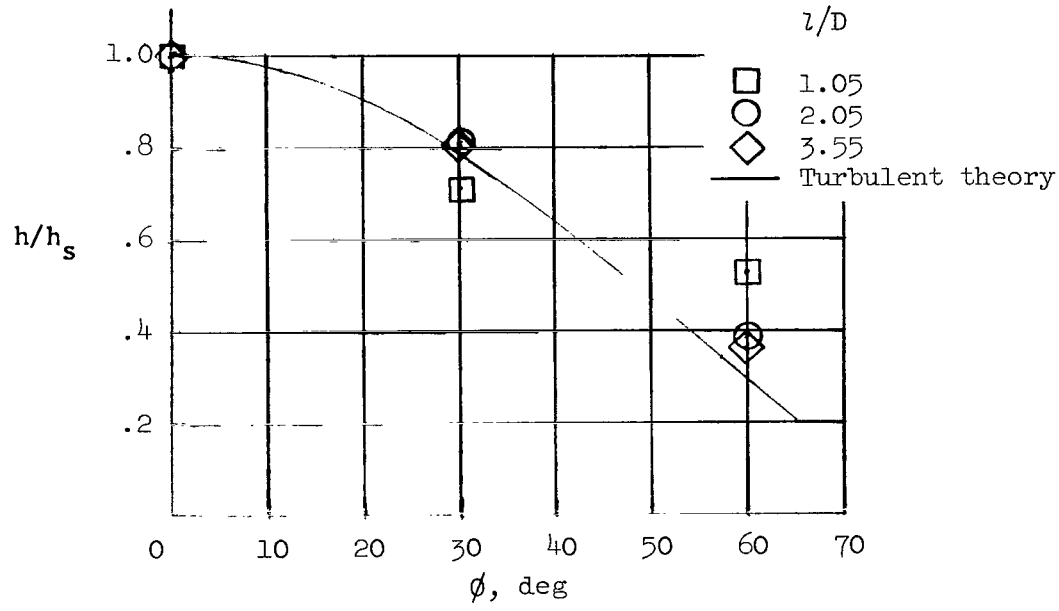

(b) $R_{\infty,D} = 2.56 \times 10^5$; $\Lambda_\infty = 60^0$.

Figure 18.- Chordwise heat-transfer distribution, cylinder only.

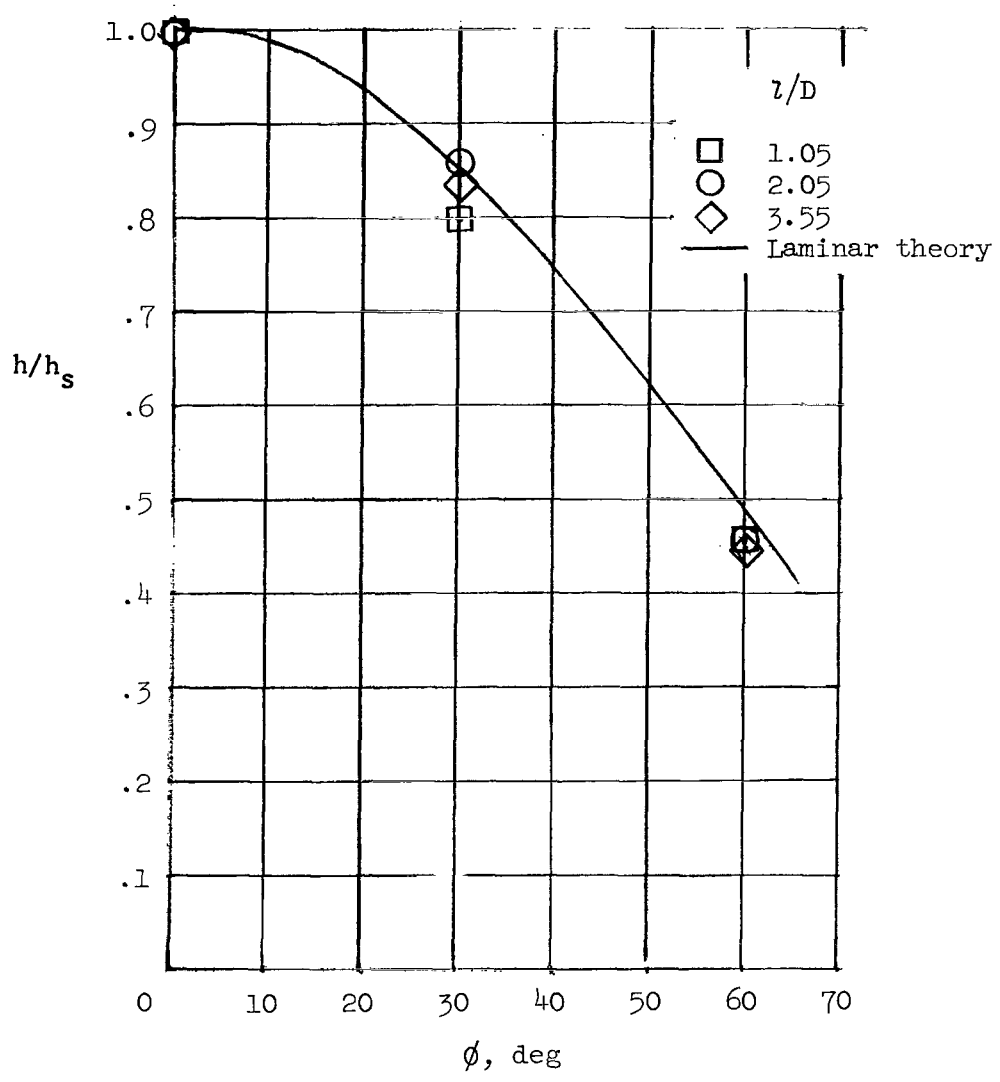

(c) $R_{\infty,D} = 1.24 \times 10^5$; $\Lambda_\infty = 45^0$.

Figure 18.- Concluded.

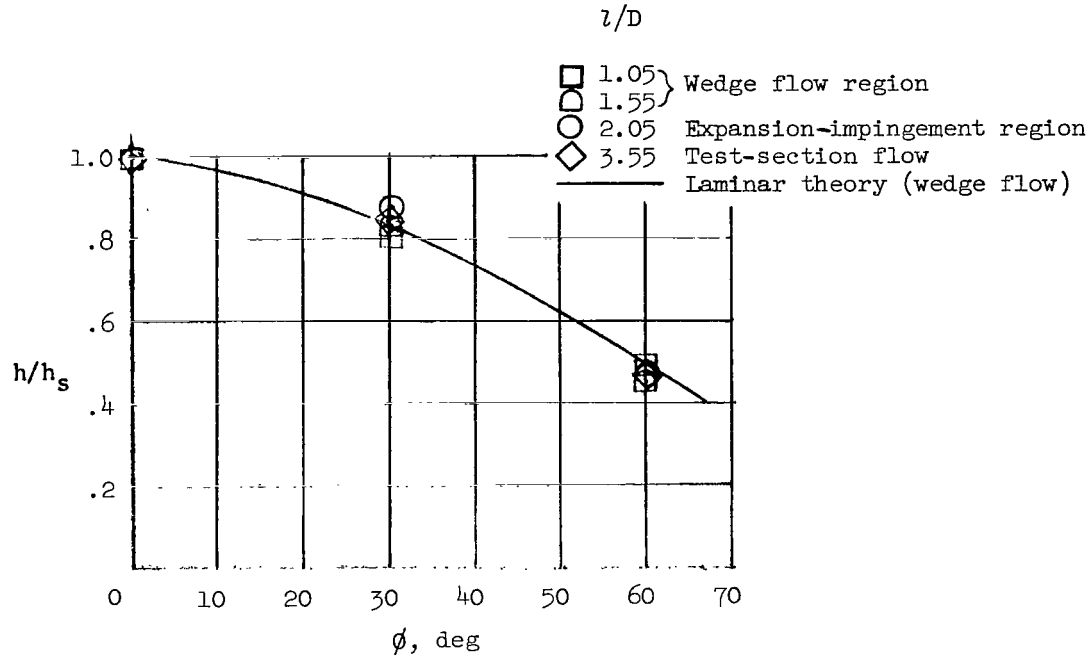

(a) $R_{\infty,D} = 0.94 \times 10^5$.

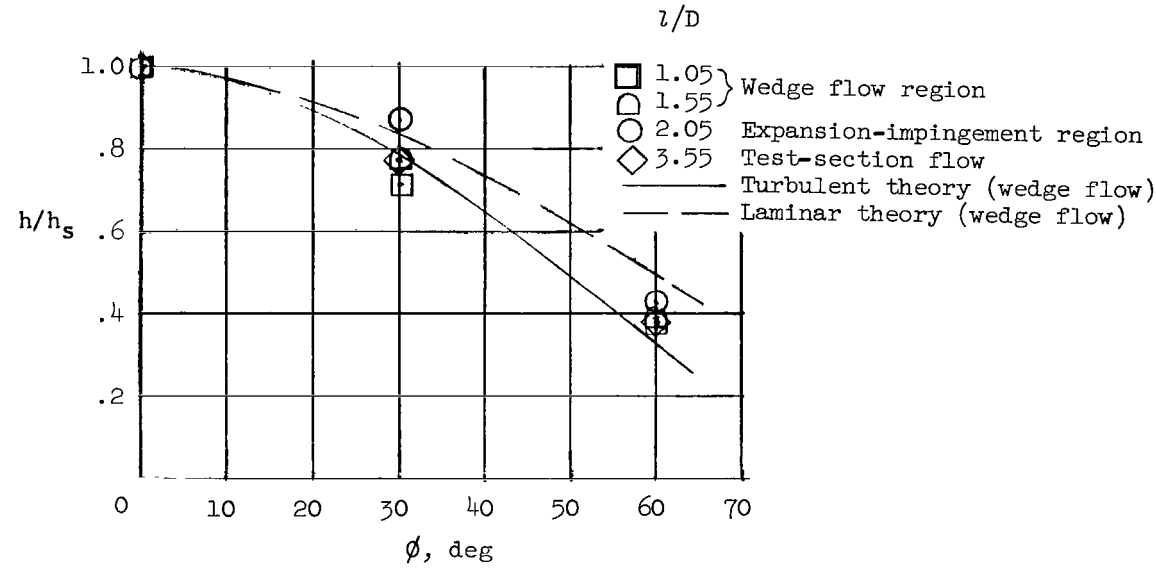

(b) $R_{\infty,D} = 1.34 \times 10^5$.

Figure 19.- Chordwise heat-transfer distribution for laminar and transitional stagnation-line boundary-layer flow, cylinder and wedge attached. $\Lambda_\infty = 45^0$.

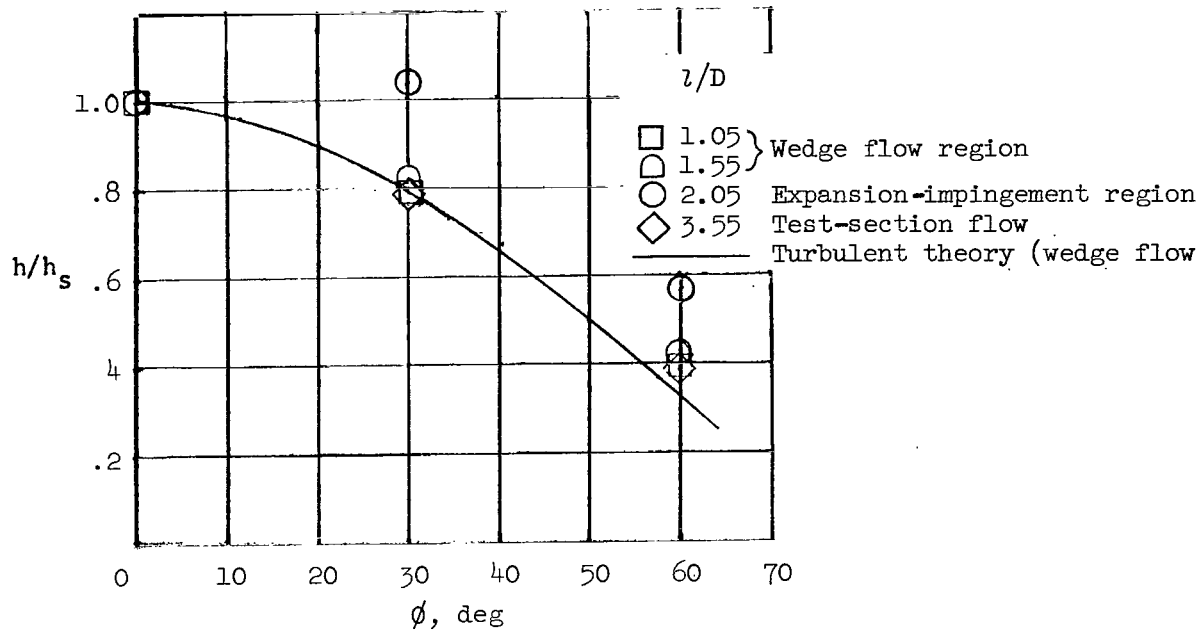

(a) $R_{\infty,D} = 2.66 \times 10^5$; $\Lambda_\infty = 45^0$.

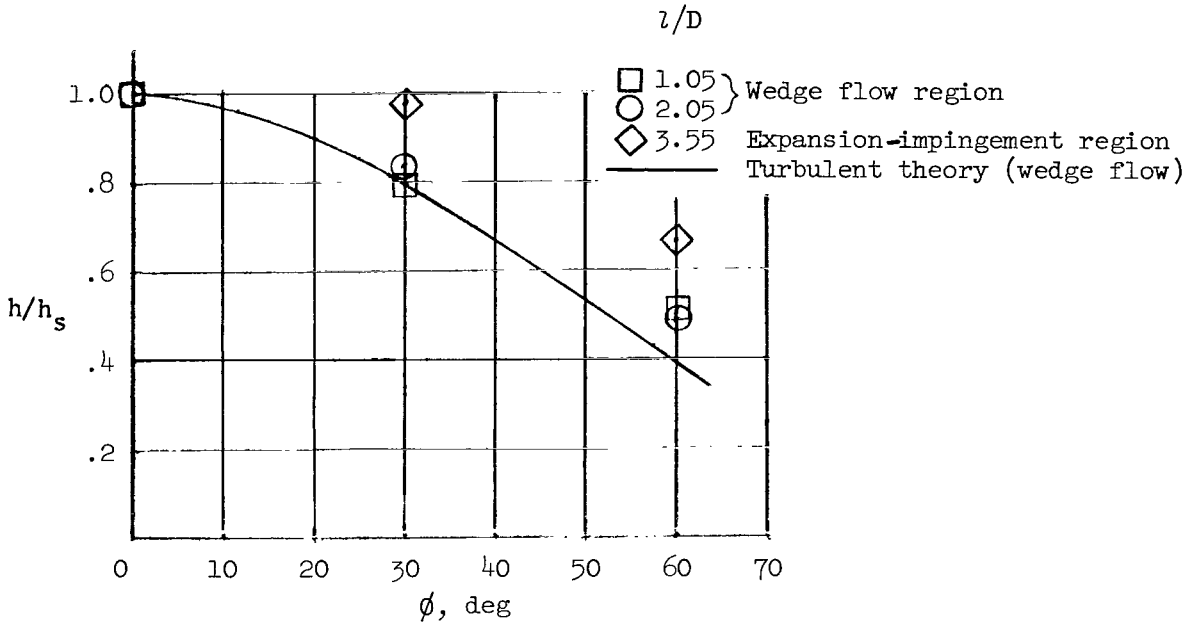

(b) $R_{\infty,D} = 2.46 \times 10^5$; $\Lambda_\infty = 60^0$.

Figure 20.- Chordwise heat-transfer distribution for turbulent stagnation-line boundary layer, cylinder and wedge attached.

3118185

"The aeronautical and space activities of the United States shall be conducted so as to contribute . . . to the expansion of human knowledge of phenomena in the atmosphere and space. The Administration shall provide for the widest practicable and appropriate dissemination of information concerning its activities and the results thereof."

—NATIONAL AERONAUTICS AND SPACE ACT OF 1958

NASA SCIENTIFIC AND TECHNICAL PUBLICATIONS

TECHNICAL REPORTS: Scientific and technical information considered important, complete, and a lasting contribution to existing knowledge.

TECHNICAL NOTES: Information less broad in scope but nevertheless of importance as a contribution to existing knowledge.

TECHNICAL MEMORANDUMS: Information receiving limited distribution because of preliminary data, security classification, or other reasons.

CONTRACTOR REPORTS: Technical information generated in connection with a NASA contract or grant and released under NASA auspices.

TECHNICAL TRANSLATIONS: Information published in a foreign language considered to merit NASA distribution in English.

TECHNICAL REPRINTS: Information derived from NASA activities and initially published in the form of journal articles.

SPECIAL PUBLICATIONS: Information derived from or of value to NASA activities but not necessarily reporting the results of individual NASA-programmed scientific efforts. Publications include conference proceedings, monographs, data compilations, handbooks, sourcebooks, and special bibliographies.

Details on the availability of these publications may be obtained from:

SCIENTIFIC AND TECHNICAL INFORMATION DIVISION

NATIONAL AERONAUTICS AND SPACE ADMINISTRATION

Washington, D.C. 20546